Remote Sensing of Environment 340 (2026) 115438

Contents lists available at ScienceDirect

Remote Sensing of Environment

journal homepage: www.elsevier.com/locate/rse

Global annual cropland dynamics 2015–2024☆

Ahmad Khan [a,*], Peter Potapov [a,b], Svetlana Turubanova [a], Matthew C. Hansen [a], Alexandra Tyukavina [a], Andrew Poulson [a], Andres Hernandez-Serna [a], Xiao-Peng Song [a], Nancy Harris [b], Fred Stolle [b]

[a] Department of Geographical Sciences, University of Maryland, College Park, MD 20742, USA
[b] World Resources Institute, Washington, DC 20002, United States of America

ARTICLE INFO

Keywords:
Cropland
Cropland change
Global land use
Landsat
Analysis-ready data
Sustainable development goals
Food security

ABSTRACT

Food security worldwide is increasingly threatened by population growth, shifting diets, geopolitical conflicts, and climate change impacts. Annual operational cropland monitoring is required to support the United Nations Zero Hunger Sustainable Development Goal. Landsat satellite data provide a foundation for such global, independent, high-cadence monitoring at 30-m spatial resolution suitable for agricultural policy and management interventions, policy responses, and market adjustments. Here, we used Landsat Analysis Ready Data developed by the Global Land Analysis and Discovery Lab (GLAD-ARD) and machine learning to map global cropland extent annually from 2015 to 2024. We showed that the global cropland area increased by more than 6% over the past decade. By combining sample-based cropland area estimates from our research and the earlier analysis (2003–2019), we estimate that the global cropland area has expanded by nearly 14% since 2003. Between 2015 and 2024, Africa accounted for the largest regional increase (+24.5 Mha). At the national scale, Brazil experienced the largest gain (+16.5 Mha) and Morocco the largest loss (−0.38 Mha). A third (33.3%) of all new cropland was established through natural vegetation clearing or irrigation expansion within natural drylands. The overall accuracies of the 2015 and 2024 cropland maps were 97.8% (Standard Error 0.3%) and 97.3% (SE 0.4%), respectively. Despite cropland expansion, population growth has outpaced cropland gains; between 2015 and 2024, per-capita cropland area declined from 0.166 to 0.161 ha per person. Our data illustrate the combined effects of changes in land use priorities, climate, water supply, international trade, and armed conflicts on global cropland extent dynamics during the last decade.

1. Introduction

Agriculture has shaped human societies and technologies for more than 10,000 years. By enabling stable food production, it supported permanent settlements, population growth, and the rise of complex societies. Over millennia, agricultural expansion became the primary force that transformed landscapes and ecosystems worldwide (Foley et al., 2005). Agricultural lands, including annual, permanent croplands, and pastures, occupy almost 40% of Earth's land surface (Ramankutty et al., 2008) and account for nearly 80% of the total human appropriation of the biosphere's net primary production (Haberl et al., 2007). During the past century, agricultural expansion and intensification have accelerated due to exponential population growth, rising per-capita consumption, globalization, and technological innovations (Lambin and Meyfroidt, 2011). Nevertheless, the global food supply still faces challenges in keeping pace with demand (WorldBank, 2023), and achieving United Nations Sustainable Development Goal (SDG) No. 2, targeting zero hunger by 2030, appears unlikely (Ackerschott et al., 2023).

Continuous expansion and intensification of crop production to meet growing demands have resulted in the loss of natural forests (Gibbs et al., 2010), the reduction of ecosystem services and biodiversity (DeFries et al., 2004; Foley et al., 2011), water scarcity, reduced environmental sustainability (Evans, 2009; Foley et al., 2005; Tilman et al.,

☆ This article is part of a Special issue entitled: 'Medium and High Resolution Satellite' published in Remote Sensing of Environment.

* Corresponding author.
E-mail addresses: akhan234@umd.edu (A. Khan), Peter.Potapov@wri.org (P. Potapov), sveta@umd.edu (S. Turubanova), mhansen@umd.edu (M.C. Hansen), atyukav@umd.edu (A. Tyukavina), apoulson@umd.edu (A. Poulson), andreshs@umd.edu (A. Hernandez-Serna), xpsong@umd.edu (X.-P. Song), Nancy.Harris@wri.org (N. Harris), Fred.Stolle@wri.org (F. Stolle).

https://doi.org/10.1016/j.rse.2026.115438
Received 11 November 2025; Received in revised form 30 March 2026; Accepted 14 April 2026
Available online 18 April 2026

2011), and increased greenhouse gas emissions (Carlson et al., 2017). These pressures highlight the intrinsic tension between the Zero Hunger (SDG 2) and Life on Land (SDG 15) goals. Moreover, cropland expansion and irrigation have also driven accelerated desertification, erosion, salinization, and precipitation changes (Becker-Reshef et al., 2010), resulting in loss of agricultural production. Urban growth, infrastructure development (Nellemann et al., 2009), climate change (Cao et al., 2021), armed conflicts (Adelaja and George, 2019; Chen et al., 2024), and economic crises (Prishchepov et al., 2013) further affect agricultural land management and productivity.

Sustainable agricultural development requires consistent monitoring of cropland dynamics and land use changes at local to global scales. Accurate and timely cropland extent and change data can inform appropriate corrective measures, policy interventions, and adjustments to market mechanisms to efficiently mitigate adverse consequences of food production shortages and land cover changes (Becker-Reshef et al., 2010; Godfray et al., 2010). Such monitoring also enables early-warning systems for addressing food security issues well ahead of a crisis (Becker-Reshef et al., 2010; Rembold et al., 2017) and supports the implementation of deforestation-free agricultural production (Heilmayr et al., 2020; Walker, 2011). Agriculture statistics collected and analyzed at the local to national levels are compiled and summarized by international organizations such as the Food and Agriculture Organization of the United Nations (FAO, 2025) and the World Bank (World Bank, 2011; World Bank, 2022). Such data, however, are often inconsistent, delayed, and/or inaccessible, limiting their usefulness for global monitoring (Boryan et al., 2011; Foley et al., 2011; Potapov et al., 2023).

Satellite-based earth observations offer opportunities for consistent monitoring of land surface dynamics, including agricultural land use. Early experiments, such as LACIE (the Large Area Crop Inventory Experiment, starting in 1974) and AgRISTARS (Agriculture and Resources Inventory Surveys Through Aerospace Remote Sensing, starting in 1980) pioneered the use of Landsat imagery and climate data from the World Meteorological Organization to map cropland extent and model crop yields (Erickson, 1984), marking the foundation for satellite-based crop monitoring (Boatwright and Whitefield, 1986). These experiments led to the development of operational agriculture monitoring systems, including the Crop Condition Data Retrieval and Evaluation system (CADRE) used by the U.S. Department of Agriculture (USDA) Foreign Agricultural Service (Reynolds, 2001) and the Cropland Data Layer (CDL) of the USDA's National Agricultural Statistics Service (USDA, 2025). Similar satellite-based crop monitoring systems have been developed by many countries, including the Monitoring of Agriculture by Remote Sensing system (MARS) of the European Union, China's CropWatch (Wu et al., 2014), and others (Becker-Reshef et al., 2010). Several global land cover maps that include a cropland class have been generated at coarse (Friedl et al., 2010; Hansen et al., 2000; Loveland et al., 2000; Pittman et al., 2010; Ramankutty and Foley, 1998) to medium spatial resolutions (Thenkabail et al., 2021; Yu et al., 2013; Zanaga et al., 2022; Zhao et al., 2025). Most of the existing global products, however, lack the capacity to accurately reflect annual spatiotemporal cropland dynamics needed for operational land management, policy implementation, and earth system modeling (Radeloff et al., 2024; Zhang et al., 2025).

The Landsat satellite constellation provides medium spatial resolution data suitable for globally consistent mapping of cropland extent at regular time intervals (Potapov et al., 2021). Annually updated cropland extent, as a separate thematic layer or as a part of the multi-class land cover and land use maps, is essential for food security and sustainable development applications (Radeloff et al., 2024). Medium spatial resolution data are especially important in regions with a predominantly smallholder agriculture land use, which cannot be adequately monitored using coarse spatial resolution imagery. As a foundational input, medium-resolution cropland maps enable a cascade of downstream products, including crop phenological monitoring, yield estimates, evapotranspiration modeling, and assessment of crop type diversity and agricultural practices. Together, these cropland extent, type, and productivity maps inform markets, government policy, and international food trade decisions, and support sustainable agricultural management and progress toward the UN SDGs (Radeloff et al., 2024). Here, we present a novel, annual, Landsat-based global cropland monitoring approach at a spatial resolution of 30 m, built upon the earlier work of (Potapov et al., 2022b). Our research had several objectives: (1) to test an efficient machine learning model calibration approach that ensures spatiotemporal consistency of the annual cropland maps; (2) to create global annual operational cropland extent monitoring tool; (3) to estimate global and regional cropland extent change during the last decade; and (4) to combine our analysis with the earlier work (Potapov et al., 2022b) to estimate cropland change over the past twenty years (2003−2023). We defined croplands as land used for annual and perennial herbaceous crop production, consistent with the FAO "arable lands" category. Following the arable land definition, we account for temporary fallows within the cropland category, limiting fallow length to four years (FAO, 2005). The Landsat Analysis Ready Dataset processed by the Global Land Analysis and Discovery team (GLAD-ARD; Potapov et al., 2020) served as the source data for our global mapping model. The GLAD-ARD consists of 16-day clear-sky normalized surface reflectance composites that were generated from the global Landsat data archive. We developed and implemented the novel locally calibrated machine-learning models designed for global annual cropland mapping for the 2015–2023 interval and demonstrated their annual update capabilities by extending the analysis to 2024. Our new mapping models show better sensitivity to cropland with a lower commission rate compared to the map by Potapov et al. (2022b), which we confirmed with independently collected reference sample data. The map and reference sample data allowed us to quantify and analyze drivers of cropland expansion and reduction over the past decade. We also combined sample-based cropland area estimates from our research and Potapov et al. (2022b) to evaluate the total change in global cropland area since 2003. The dataset and operational machine learning mapping approach presented here provide globally consistent data needed to inform SDG targets that balance zero hunger with ecosystem services protection.

2. Methods

2.1. Area of analysis and cropland definition

To ensure that our dataset is comparable with other global cropland maps, we performed the analysis within 13,451 1 × 1 geographic degree grid cells that contain croplands mapped by either U.S. Geological Survey (USGS) Global Food Security-support Analysis Data at 30 m (GFSAD) (USGS, 2023) or global cropland map (Potapov et al., 2022a). Small islands were excluded because terrain-corrected Landsat data do not cover these areas. The analysis extent map is presented in Supplementary Fig. 1.

The source Landsat data (GLAD-ARD) and the output maps share the same global pixel grid with the spatial resolution of 0.00025 degrees per pixel (~30 m per pixel on the Equator). We used geographic coordinates defined using the WGS84 datum (World Geodetic System 1984, EPSG:4326) to store and process data, which simplified global data aggregation, cropland mapping, and product visualization. Because the area of each pixel in geographic coordinates changes with the latitude, we used the equations from Tyukavina et al. (2025, Appendix D) to correctly calculate map-based areas of the cropland product.

Our cropland definition is closely related to the FAO arable land category (FAO, 2024) and the cropland category from Potapov et al. (2022b). We defined croplands as land used to grow annual and perennial herbaceous crops for human consumption, forage, or biofuel. We excluded perennial woody crops, tall non-woody perennial crops (such as bananas), permanent pastures, and shifting cultivation. Similar to the FAO arable lands definition, our cropland definition includes

temporary fallows, provided the fallow period did not exceed 4 years. Unlike the FAO definition, we do not include temporary meadows and pastures unless they represent a short phase between row crop production cycles. Land used for hay production, if regularly tilled and planted, is included in our cropland category.

2.2. Landsat analysis ready data

Globally consistent Landsat Analysis Ready Data processed by the Global Land Analysis and Discovery team (GLAD-ARD; Potapov et al., 2020) served as the input features for annual cropland mapping. To create GLAD-ARD, we used all available 2015–2024 Landsat Collection 2 archive data from 6694 World Reference System-2 (WRS) scene footprints that cover our analysis area (Supplementary Fig. 1). The source Landsat images were available from the U.S. Geological Survey Earth Resources Observation and Science Center (USGS EROS; https://earthexplorer.usgs.gov/).

We processed Level 1 Tier 1 (L1TP) top-of-atmosphere reflectance (TOA) terrain-corrected images. Images during the snow-covered season in the temperate climate zone were excluded using the approach of Potapov et al. (2020), which identified snow-covered season dates for each WRS scene using the Moderate Resolution Imaging Spectroradiometer (MODIS) snow cover monthly global product (https://nsidc.org/data/MOD10CM/versions/6). Images with near-complete cloud cover that precluded data normalization were also excluded. Overall, we used 698,729 Landsat 7 Enhanced Thematic Mapper Plus (ETM+) images and 1,351,087 Landsat 8 and 9 Operational Land Imager and Thermal Infrared Sensor (OLI/TIRS) images. The average number of images per year was ~200,000. From 2015 (Landsat 7 and 8) to 2024 (Landsat 8 and 9), the number of images per year increased by 2.7%, which did not introduce significant bias in data availability between years.

Each selected Landsat L1TP image was automatically processed into normalized surface reflectance data. The processing workflow included two steps: observation quality assessment and data normalization. The objective of observation quality assessment was to attribute each pixel within the Landsat image to clear-sky (separated into land, water, and snow land cover) and cloud-contaminated (including clouds, haze, and cloud shadows). We applied a set of purposefully calibrated decision tree models to attribute per-pixel observation quality and land cover type, and merged model outputs with the Quality Assessment (QA) of the L1TP product. After the clear-sky land pixels were selected, we performed reflectance normalization to reduce the effect of radiation scattering and attenuation by the atmosphere and surface anisotropy. We used the annual growing season reflectance composite derived from the MODIS MOD44C 6-day surface reflectance product at a spatial resolution of 250 m. We employed 10 years of MODIS data to create a single global image composite to ensure long-term data consistency. We calculated the bias between Landsat TOA and MODIS surface reflectance for each spectral band within clear-sky land pixels that had the difference between Landsat and MODIS reflectance values below 0.1 to remove areas affected by recent land cover change. We then modelled this bias for each spectral band as a function of the Landsat scan angle to account for surface anisotropy. The modelled reflectance bias was then calculated for each data pixel and applied to the entire Landsat image. While the normalized surface reflectance calculated for each Landsat image is not equal to the surface reflectance provided by the Landsat Level 2 products, it is closely related to surface reflectance (Potapov et al., 2020), and our earlier work confirmed its ability to provide spatiotemporally consistent inputs for global land cover and land use mapping (Potapov et al., 2022a).

After surface reflectance normalization, individual Landsat 7, 8, and 9 images collected during each 16-day interval were composited, prioritizing clear-sky observations. The Landsat images were reprojected using the nearest neighbor resampling method into geographic coordinates (EPSG:4326) to simplify global data handling. For each pixel of the 16-day composite, we selected the Landsat image with the best quality from all observations available during this time interval. Each 16-day composite includes the spectral data from six bands: blue (482 nm), green (561 nm), red (654 nm), near-infrared (NIR, 864 nm), shortwave infrared 1 (SWIR1, 1609 nm), and SWIR2 (2201 nm); the brightness temperature, and observation quality flag. To simplify data distribution and parallel processing, the GLAD-ARD product uses a 1 × 1 geographic degrees tile system (Potapov et al., 2020). The GLAD-ARD data is provided online and is freely and publicly available without restrictions (https://registry.opendata.aws/glad-landsat-ard/).

2.3. Spectral-temporal features for cropland mapping

To improve cropland detection, we enhanced the representation of land surface phenology by combining GLAD-ARD data from each analysis year with data from the three preceding years. Aggregating four years of data increases the number of clear-sky observations during growing season, enabling cropland detection even in persistently cloudy regions. This approach also simplifies the enforcement of a maximum 4-year fallow interval in the combined time-series, we selected the clear-sky observation with the highest near-infrared (NIR) reflectance across the four years, prioritizing observations with dense vegetation cover. As a result, if a crop was cultivated at any point during the past four years, our features will capture it. However, this also means that crop abandonment detection is delayed, since the selected observations will continue to reflect past cropping activity for up to four years after abandonment.

The analysis of clear-sky data availability over 10 years within the area of analysis showed that 77% of the land area had at least 12 clear-sky 16-day composites per year. Only 0.5% of the land within the area of the analysis had no clear-sky observations during at least one year. Such areas usually represent permanently bright objects, such as dense urban areas, glaciers, high deserts, and salt pans, where the observation quality model overestimated cloud presence. The lack of clear-sky observations within such areas did not affect our cropland mapping.

If no clear-sky observations were available for a given interval, the 16-day reflectance values were linearly interpolated between the closest consecutive clear-sky observations. This approach produced a continuous, gap-free 16-day time series for each analysis year. We excluded the 16-day intervals during seasonal snow cover in temperate regions using the approach of Potapov et al. (2020), because these data are irrelevant for cropland detection.

For each 16-day composite, we included the spectral data from six bands (see Section 2.2) and brightness temperature. Additionally, we calculated a set of indices using the input spectral bands, including normalized ratios of NIR and red bands (Normalized Difference Vegetation Index, NDVI; Tucker, 1979), NIR and green, NIR and SWIR1 (Normalized Difference Water Index, NDWI; Gao, 1996), NIR and SWIR2 (S2N), and SWIR1 and SWIR2 bands (Normalized Difference Tillage Index, NDTI; Van Deventer et al., 1997), the Spectral Variability Index (SVVI, Coulter et al., 2016), and the Tasseled Cap Greenness component (DeVries et al., 2016).

The resulting 16-day time series for each year were transformed into a set of spectral-temporal features that provide consistent land-surface phenology inputs for global cropland mapping. We extracted three distinct types of spectral-temporal features (Supplementary Table 1) following the approach prototyped by Potapov et al. (2020, 2021). The annual spectral reflectance distribution and trend features represent statistics extracted from the twenty-three 16-day intervals within each year. For each spectral band and index, we calculated descriptive statistics (minimum, maximum, mean, and median), interquartile averages (i.e., the mean of all values falling between the first and third quartiles), range statistics (total range and interquartile range), and mean absolute difference between consecutive 16-day observations within the year. The annual seasonality features represent statistics extracted from the

16-day spectral reflectance values ranked by the corresponding vegetation indices (NDVI and S2N) and surface temperature values. To calculate these features, we first distributed 16-day interval dates according to the value of the corresponding variable. We then extracted the value of each spectral band that corresponds to selected ranks of the corresponding variable, e.g., red surface reflectance for the observations with the maximum and minimum NDVI values. The annual phenology features were extracted from the NDVI time series. First, we defined the dates of the start and end of the growing season that represented the start of the NDVI increase toward the annual maximum and the end of the NDVI decrease after the maximum. We recorded the 16-day interval date and calculated NDVI amplitudes between the maximum value and the start and end season values, and the slope of NDVI increase and decrease. We also calculated the sum and average of all NDVI values from 16-day composites during the growing season. In addition to the features calculated per pixel, we also calculated the average feature value within a 3 × 3 pixel area around each pixel to provide spatial variation information to the machine learning model. The GLAD-ARD-based annual features were augmented with elevation data (Jarvis et al., 2008). The total number of spectral-temporal and elevation features and their local averages for each year and each pixel was 546.

An analysis of feature importance for 2003–2019 global cropland mapping (Potapov et al., 2022b) and visual assessment of image composites suggested that some spectral-temporal features were particularly effective for cropland identification. Specifically, red, NIR and SWIR bands, along with indices such as NDVI, NDTI, and Tasseled Cap Greenness, had high explanatory value. Spectral reflectance corresponding to the maximum NDVI was particularly useful because it highlights the spectral properties of the vegetation during the peak of the growing season, independent of the date of maximum greenness in each particular pixel. Among the different statistics extracted from the 16-day time series, we found that the average absolute difference can highlight the intrinsic spectral dynamic properties of the cropland: high reflectance amplitude, fast change of reflectance during the year, and the contrast between the spectral reflectance during peak greenness and soil tillage or crop senescence phases. Some of these features were combined into the RGB (red-green-blue) visual composites to support cropland mapping and map evaluation (Fig. 1).

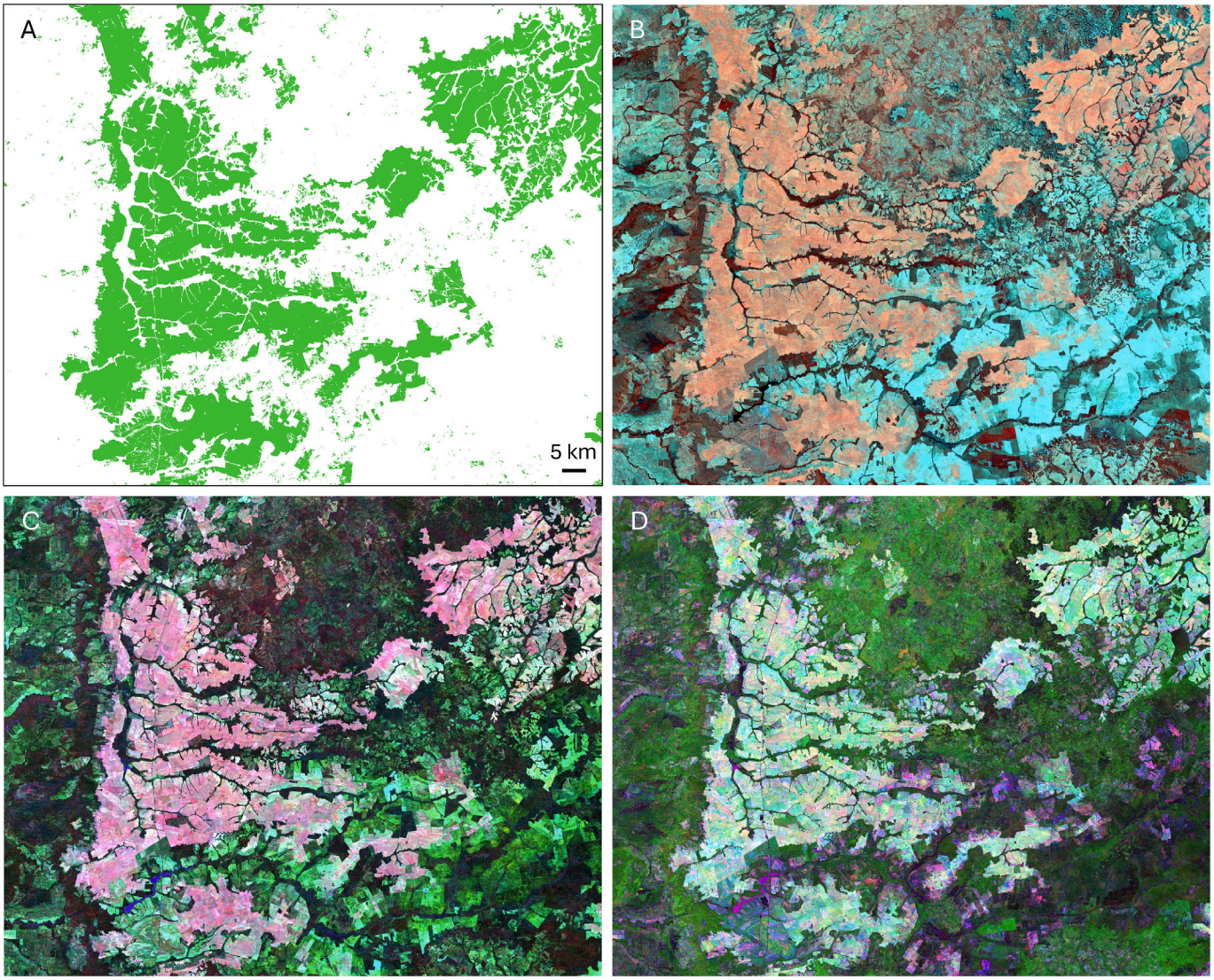

Fig. 1. (A) The year 2024 cropland extent within the Brazilian state of Mato Grosso do Sul, centered at 17°W; 54.5°S, and year 2024 RGB composites of Landsat spectral-temporal features used for cropland detection: (B) NIR, SWIR1, and SWIR2 average reflectance from 16-day composites with NDVI between 75th percentile and the maximum annual value; (C) the average absolute difference of NIR, SWIR2, and NDVI values between all consecutive 16-day composites within the year; and (D) an RGB composite of the start of season slope of NDVI increase (red), maximum annual Tasseled Cap Greenness (green), and average absolute difference of NDVI values between all consecutive 16-day composites within the year (blue). (For interpretation of the references to colour in this figure legend, the reader is referred to the web version of this article.)

2.4. Global cropland mapping

Our cropland mapping approach relies on regionally calibrated ensembles of decision tree models. Restricting each model to a local region simplifies its calibration and improves precision (Potapov et al., 2022a; Potapov et al., 2021). For the global mapping, we delineated 45 geographic regions with similar dominant crop types, crop calendars, and spatial distribution of croplands within the landscape (Supplementary Fig. 1). We independently calibrated a cropland mapping model for each of these regions.

The model calibration was conducted using an interactive learning approach. First, an analyst manually collected training data representing cropland presence and absence. These training data were used to calibrate the model, and the results were visually evaluated by the analyst. If the analyst identified mapping errors, new training data were manually added to the pool, and the model calibration was repeated. This iterative process continued until the analyst determined that the map quality was satisfactory.

Training data for model calibration were collected manually using Landsat features composites (Fig. 1) and high-resolution imagery from Google Earth. To simplify the delineation of training areas and to improve the consistency between the newly created map and existing products, we used several reference datasets, including European Space Agency (ESA) WorldCover 2021 (Zanaga et al., 2022) and the 2021 USDA Cropland Data Layer (USDA, 2025). In addition, we implemented the Potapov et al. (2022b) cropland model for the year 2021 and used the output as a reference. An analyst evaluated the reference products using the Landsat features composites and, if a particular product was considered sufficiently accurate, delineated cropland and no cropland extent from this product to be included in the training dataset. If none of the products were considered accurate, the analyst manually collected training data (cropland presence and absence) through visual interpretation of Landsat and high-resolution imagery. In this way, we quickly collected an average of 50 million training samples (Landsat pixels) for each regional model.

Each regional model consists of an ensemble of 25 decision trees, each calibrated with a 1% random subset of the training population. The decision tree ensemble approach reduces overfitting to errors in the calibration data and inconsistencies in spectral-temporal features (Breiman, 1996). The average number of training samples (Landsat pixels) per decision tree was 0.5 million. Each of the decision tree models used in regional ensembles explained on average 86% of the root deviance. The most important spectral-temporal features for all 45 regional models were the amplitude of the NIR/SWIR2 normalized ratio, red band reflectance corresponding to the peak NDVI and to the minimum land surface temperature during the year, maximum value of NDTI, and elevation. While the decision tree model does not allow us to evaluate the physical reasons for feature selection, we suggest that elevation allowed partitioning of the regional area into sub-regions with different spectral properties of croplands, maximum NDTI values indicated tillage and crop harvesting, and NDVI-based observation date ranks allowed extraction of spectral data during the peak crop growing stage. The local averages of the Landsat spectral-temporal features were responsible for 85% of the total explained deviance, illustrating the importance of spatial context in cropland mapping.

We calibrated each regional model in two steps. In the first step, we used 2021 Landsat spectral-temporal features and image composites to collect training data and map the 2021 cropland extent. In the second step, we applied the 2021 model for each year from 2015 to 2023. We assessed the results and added training samples in areas where annual model performance was unstable, resulting in false cropland gain and loss detections. The new training data were extracted from the years affected by the model instability and added to the 2021 training pool to recalibrate the model and improve its performance. The final model was applied for all years, 2015–2023.

In addition to the new cropland mapping model, we applied the model developed by Potapov et al. (2022b) to improve consistency between the 2003–2019 and 2015–2023 products. This model consists of a set of decision tree ensembles calibrated locally and independently for each $1^\circ \times 1^\circ$ grid cell using the same Landsat spectral-temporal features. Although this model was calibrated at 4-year intervals, here we applied it annually.

At the final step of cropland mapping, we combined annual outputs using temporal filtering to ensure map consistency between years. Temporal filtering rules included filling gaps in cropland detection of up to three years, consistent with the 4-year fallow definition, and removing single-year cropland detections not confirmed by crop presence in the two preceding and two following years. Spatial filtering rules included removing narrow (1 pixel wide) strips and single cropland pixels separated from larger patches. Manual masks to remove map artifacts (for example, cropland overestimation over temperate wetlands and flooded grasslands) were applied in some regions to improve map quality. The importance of temporal filtering highlights that the automated classification alone did not capture the full complexity of cropland dynamics, and that additional temporal and spatial post processing, along with targeted manual corrections, helped us to enhance map consistency and accuracy.

We defined cropland change classes directly from the filtered annual cropland time series. Stable cropland and no-cropland classes include pixels with the same map value for all years, 2015–2023; net cropland gain and loss were defined as pixels with a single transition during the 2015–2023 interval; the remaining pixels that represent crop abandonment and re-cultivation during the 2015–2023 interval were classified as the irregular cropland dynamics category. After producing the maps of cropland change types, we applied an additional spatial filter to reclassify narrow (1-pixel-wide) change areas adjacent to stable cropland patches into the stable cropland category. We considered that such narrow change areas, in most cases, represent mixed pixels with unstable annual model outputs. Finally, we combined the new maps with the Potapov et al. (2022b) model outputs to harmonize the two products. This step was guided by manually delineated masks to select a few localized areas where we observed inconsistencies between the maps. Within such areas, we considered cropland areas mapped by either of the two models.

After creating a time series of annual cropland maps for 2015–2023 and validating this product, we applied the same classification model to the 2024 Landsat spectral-temporal features to update the global product for the 2015–2024 interval and to demonstrate the operational update capabilities of the proposed method. A simplified version of spatiotemporal filtering was applied to detect cropland expansion and reduction compared to 2023. The final 2015–2024 global cropland map time series is publicly available from https://glad.umd.edu/dataset/annual-croplands.

2.5. Sample analysis

The objectives for the cropland extent and change sample analysis were to (i) estimate the area of global cropland extent for the years 2015 and 2023, comparable to the sample-based estimates of Potapov et al. (2022b), (ii) assess accuracy of the new annual cropland extent and change maps at the global-scale, and (iii) quantify global land use trajectories of cropland change. Our sampling analysis approach is based on the global sampling design and estimators described in Tyukavina et al. (2025), Appendix A.1.1. The Landsat GLAD-ARD data pixel ($0.00025^\circ \times 0.00025^\circ$) represented our sampling unit. The entire area of analysis (Section 2.1) was used to define a sampling population. We implemented a stratified sampling design with six strata (Table 1) to target the areas of cropland presence and absence, cropland extent change, and areas of potential cropland commission and omission, following recommendations of Olofsson et al. (2020). The potential cropland omission stratum was selected within the 2015–2024 non-cropland area using the following criteria: (i) a 1-pixel boundary from

Table 1
Stratification and sampling design.

Strata	Stratum size, pixels (N_h)	Sample size, pixels (n_h)
Stable cropland	15,101,549,966	112
Net cropland gain 2015–2024	1,916,393,485	250
Net cropland loss 2015–2024	1,131,689,231	250
Stable non-cropland	28,673,763,006	108
Potential cropland omission	164,320,002,569	182
Potential cropland commission	4,072,601,743	37

cropland presence; (ii) cropland presence indicated by GFSAD or ESA WorldCover 2021 products. The potential cropland commission stratum is a post-stratum within the stable cropland stratum that includes pixels within 30 m of the edge of cropland patches. The initial sample allocation was guided by the sample variance obtained from the sample data of Potapov et al. (2022b) within our strata. The sample size was increased for net cropland loss and gain strata to enable the analysis of cropland change land use trajectories. Overall, we randomly selected 939 pixels. The total number of samples was limited by the project's scope and funding.

Samples were visually interpreted using available remotely sensed data time series, including GLAD-ARD 16-day composite data, composites of selected spectral-temporal Landsat features, high-resolution images provided by Google Earth, and Planet monthly base maps. We employed the same cropland identification criteria and cropland change trajectory classes as in Potapov et al. (2022b) to ensure compatible and consistent estimates. For each sample, we recorded: (1) cropland presence for the year 2015 and 2023; (2) cropland expansion and abandonment between 2015 and 2023; and (3) the type of land-use trajectory (see Table 5 for the trajectory types). Each sample pixel was interpreted by two experts independently and reviewed by a third expert. Sample interpretation disagreements were discussed and resolved by the research team.

We estimated the global cropland areas for the years 2015 and 2023 and their associated uncertainties using equal probability sampling equations from Tyukavina et al. (2025), Appendix A.1.1. We also estimated the sample-based proportions of the correctly mapped net cropland loss and gain classes attributed to different land use trajectories. This way, we produced the global estimates directly comparable to the 2003–2019 estimates of Potapov et al. (2022b). The map accuracy metrics include overall accuracy (the proportion of the total map area that is correctly mapped), user's accuracy of the cropland class (which reflects the cropland class commission), and producer's accuracy of the cropland class (which reflects the cropland class omission). The map accuracy metrics, along with their standard errors, were estimated using equations from Tyukavina et al. (2025), Appendix A.1.1.

3. Results

Using our cropland extent maps, we estimated a 6% increase in global cropland area over the past decade, from 1238 Mha in the year 2015 to 1312 Mha in the year 2024. Our map-based estimates closely agree with the sample-based cropland area estimates of 1221 ± 95 Mha (95% confidence interval) for the year 2015 and 1301 ± 107 Mha for the year 2023. Sample analysis confirmed the high accuracy of the 2015 and 2023 cropland extent maps, with overall accuracies exceeding 97% and balanced user's and producer's accuracies (Table 2). The mapped annual cropland area increased nearly linearly over the last decade, with an average annual increase of 8.2 Mha/year (Fig. 2A). The sample estimates suggest a slightly higher annual increase of 9.9 Mha/year between 2015 and 2023. Both estimates exceed the 6.4 Mha/year estimated by Potapov et al. (2022b) for the 2003–2019 interval using sample data, suggesting continued acceleration of global cropland expansion.

Table 2
Accuracies of the cropland extent and change maps. Accuracy metrics are expressed as a percentage, and standard errors are shown in parentheses.

	Cropland 2015	Cropland 2023	Cropland loss	Cropland gain
Overall	97.8 (0.3)	97.3 (0.4)	99.7 (0.1)	99.2 (0.2)
User's	87.7 (2.2)	86.0 (2.3)	62.8 (4.2)	64.8 (3.4)
Producer's	87.5 (2.7)	84.7 (2.9)	40.7 (12.6)	47.3 (9.7)

Our sample-based estimates are consistent with the 2003 and 2019 estimates published earlier (Potapov et al., 2022b, Fig. 2B). However, the earlier 4-year interval map underestimated cropland extent compared to the sample-based estimates. Using our sample data, we estimated the accuracy of the 2015 map published by (Potapov et al., 2022b). We found that the past map had a lower overall (96.9%, Standard Error 0.4%), user's (85.0%, SE 2.7%), and producer's (78.8%, SE 3.3%) accuracies. The imbalance between the user's and producer's accuracies indicates map omission, which resulted in cropland area underestimation compared to reference sample-based estimates. By contrast, our updated product outperforms the Potapov et al. (2022b) cropland mapping method, producing a map with higher accuracy and better agreement with the reference sample data.

We estimated an overall 13.8% increase in global cropland area by comparing the year 2003 (Potapov et al., 2022b) and our new 2023 sample-based estimates (Fig. 2B). A slightly higher increase (14.9%) is observed when adding the net change computed from the year 2003 and 2015 cropland maps (Potapov et al., 2022b) to the net change 2015–2024 computed using our new cropland maps. A consistent increase in cropland area during the last decade (Fig. 2A) indicates that, assuming the recent linear trend continues, global total cropland area would reach 1526 Mha by 2050, a nearly 35% increase compared to 2003.

Map accuracies for gross cropland change dynamics were lower than for cropland extent maps (Table 2). The higher user's accuracies compared to the producer's accuracies suggested that gross change dynamics are underestimated. We analyzed the main sources of errors using sample pixels where the map disagrees with the reference. Of all sample pixels with disagreement, the majority was due to confusion of actively managed croplands with intermittent fallows and pastures (38% of all sample pixels with disagreement), border or mixed pixels (25%), and drylands with irregular crop production (10%). Agroforestry, especially fast-rotating permanent crops such as bananas and berries, was responsible for 9% of all errors. Pixels where changes were observed in the first (2015) or last (2023) year and were omitted from the map contributed 5% of disagreement pixels. These artifacts are due to the use of 4-year aggregated Landsat data, which delays the detection of crop abandonment and conversion. Most of the sample pixels with errors were found in Africa and Asia (56% of the total), followed by Europe (24%). North America, South America, and Australia together contained 21% of the total sample pixels with disagreement. This observation is consistent with the finding by Potapov et al. (2022b) that the Landsat-based mapping methods tend to have lower accuracy in drylands and smallholder agriculture landscapes (where low crop productivity and landscape heterogeneity limited the mapping model sensitivity) compared to industrial agriculture areas.

The global cropland area distribution map for the year 2024 (Fig. 3A) highlights regions with the most intensive annual cropland production. These regions include the Great Plains and Central Lowlands of North America, the Pampas and Mato Grosso Plains of South America, the European steppe, the Sahel and Eastern Africa, India, Indochina, the Chinese and Manchurian Plains, and Eastern Australia.

To illustrate the spatial distribution of the global cropland change from 2003 to 2024, we summarized the map-based net cropland area change between 2003 and 2015 using the map of Potapov et al. (2022b) and the net change from 2015 to 2024 using the new map time series (Fig. 3B). While these maps may have differences, we considered that the combination of the net changes mapped by both products represent the only viable method to illustrate the spatial pattern of the global

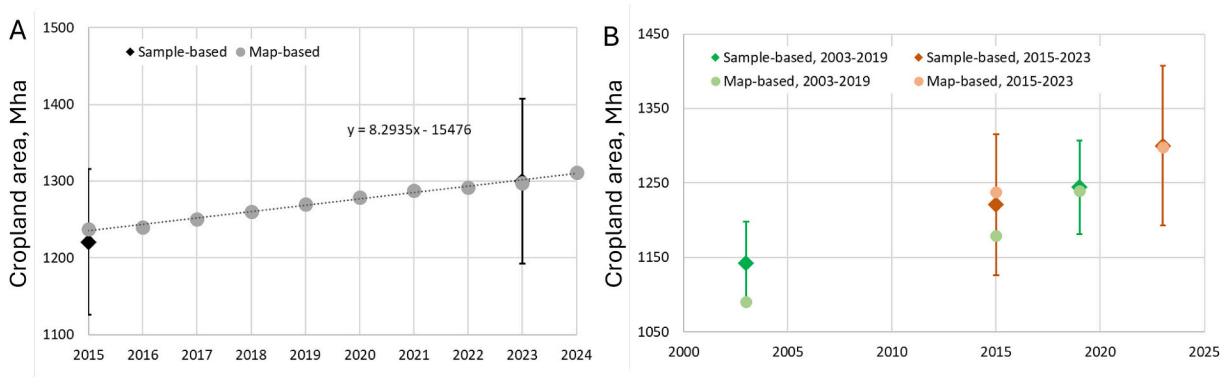

Fig. 2. A. 2015–2024 map-based and sample-based global cropland area, Mha. B. 2003–2019 map-based and sample-based estimates from Potapov et al. (2022) in comparison with the 2015–2023 estimates from the current research. The sample-based estimates are shown with a 95% confidence interval.

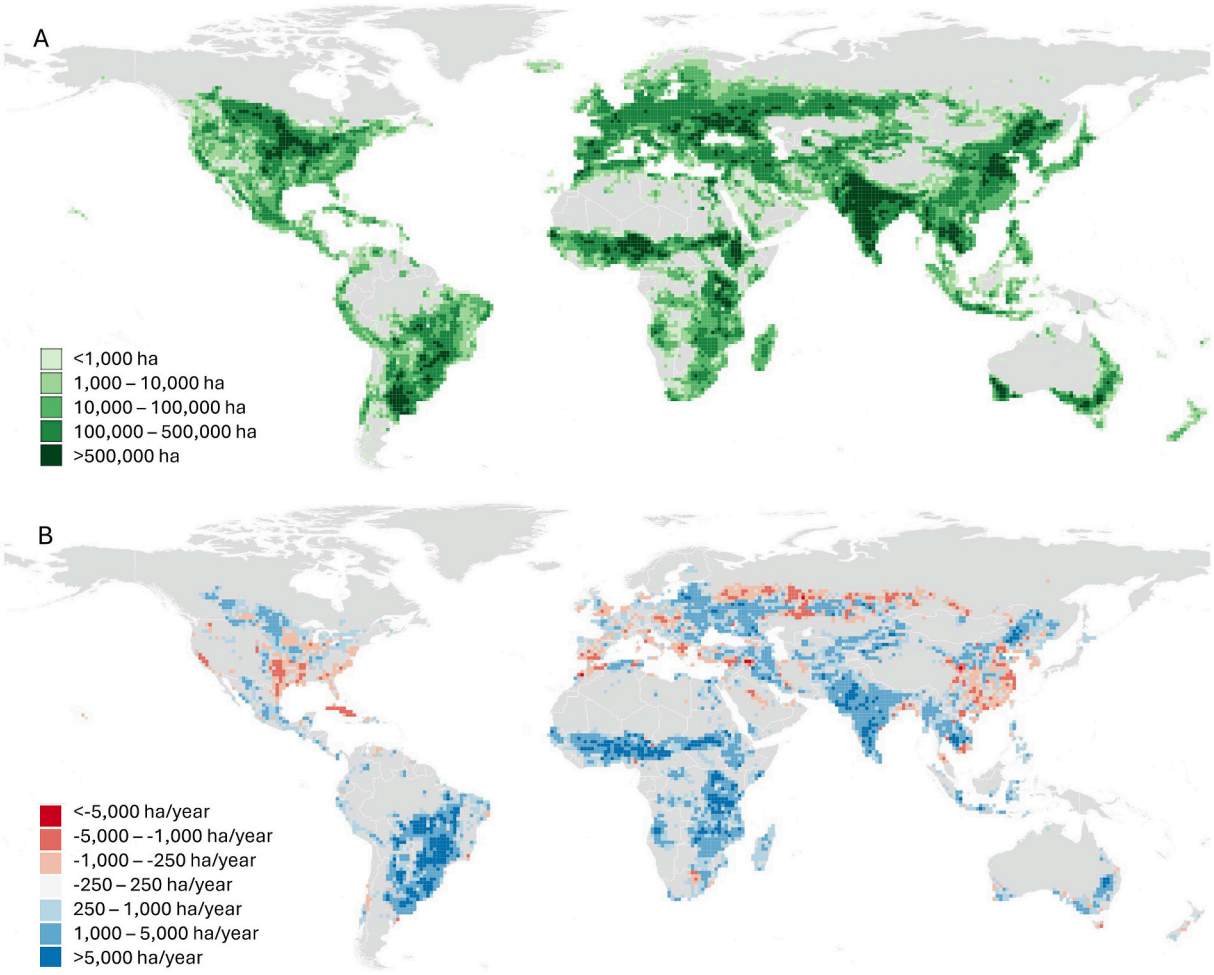

Fig. 3. Cropland extent and change area for each 1° × 1° tile. A. Total cropland area, 2024. B. Net cropland area change, 2003–2024. The net cropland area change was derived by adding the net change computed from the year 2003 and 2015 cropland maps (Potapov et al., 2022b) to the net change 2015–2024 computed using our new cropland maps.

multidecadal cropland area changes. The net cropland gain areas highlighted regions and countries with fast agro-industrial development and/or population growth, such as Brazil and Argentina in South America, the Sahel and East African countries, India, and China. Eastern European countries, including the southern part of European Russia, also experienced net cropland gain over the past decades due to the re-cultivation of the agricultural lands abandoned after the collapse of the soviet economies in the early 1990s. We observed the continuous expansion of agriculture within subtropical woodlands and drylands, including commercial land use conversion and irrigation (Brazil and China) and smallholder cropland expansion (Africa, Southwest, and Southeast Asia). By contrast, the largest hotspots of cropland loss were found in China as a result of urbanization and cropland conversion to tree crops and aquaculture. The other cropland abandonment hotspots were in the northern parts of the agricultural belt in Russia, where crop production is less profitable. We also observed a reduction in cropland

area in Cuba and most Western European countries. In North America, cropland area is declining in the South and southern Midwest states of the USA, while it is increasing in the northern part of the Great Plains in the USA and Canada.

3.1. Cropland area and change at the continental, national, and administrative levels

We analyzed cropland change at the continental scale using the continental boundaries from Potapov et al. (2022b) for consistency (Table 3). In 2024, three continents, Southwest Asia, Europe (including Russia), and Africa, had the largest share of global cropland, together accounting for more than half (57%) of the global cropland area. During the last decade, cropland area expanded most rapidly in South America (17.4%) and Africa (12%), while cropland extent in North America remained stable. For most continents, annual cropland expansion rates were similar to those observed during 2003–2015. The fastest annual increase occurred in Africa (by 2.7 Mha/year), followed by South America (2.2 Mha/year). The only continent with a significant transition in cropland dynamics was Europe (including Russia), which changed from a small net cropland loss (2003–2015) to a substantial net cropland gain (2015–2024), resulting in an overall net increase of cropland area from 2003 to 2024.

In 2024, fifteen countries with the largest cropland extent accounted for 68% of the global cropland area (Table 4). Nearly one-third of the total global cropland area was concentrated within just three countries: India, China, and the United States. Most countries showed stable or increasing cropland area during the last decade (Fig. 4). Brazil had the largest net cropland area increase (16.5 Mha), followed by Russia, India, China, and Tanzania, each with gains exceeding 3 Mha. Over the past two decades, Brazil has more than doubled its cropland area, standing out among all countries as the single largest contributor to global cropland expansion. Other notable increases since 2003 include Argentina and the African nations of Nigeria, Sudan, and Tanzania, each with more than 20% cropland increase between 2003 and 2024.

In contrast, seven countries experienced net cropland area reductions of at least 0.1 Mha. The largest losses were observed in Morocco (−0.38 Mha) and Germany (−0.23 Mha). Smaller declines of 0.1–0.2 Mha occurred in several European countries (the United Kingdom, France, Denmark), Cuba, and the United States. Among these, only Cuba experienced a net cropland area reduction during the preceding 2003–2015 interval.

Out of the seven countries with the largest cropland extent in 2024, Brazil and China featured accelerated annual cropland expansion during the last decade (Fig. 5). Brazil has consistently led global cropland expansion for more than two decades and continues to expand at the fastest rate worldwide. In contrast, India, Argentina, and Australia reduced their cropland expansion rates during the last decade, but these countries have kept expanding their cropland areas. The USA has maintained a nearly stable cropland area for several decades, with insignificant changes. Russia presents a distinct trajectory: it experienced the largest net cropland loss between 2003 and 2015 (Potapov et al., 2022b), but reversed this trend in the last decade, achieving a net cropland gain over the full 2003–2024 period.

Using the country-level cropland statistics presented above, we also evaluated the consistency of our maps against other global products. We compared our 2021 cropland map with the cropland layer from the 10 m spatial resolution ESA WorldCover 2021 (Zanaga et al., 2022). The country-wise cropland extent from our study corresponds well to the area estimates of Zanaga et al. (2022) with a R^2 of 0.995 (Fig. 6).

To better understand within-country dynamics, we next examined cropland change at the sub-national level, within large agricultural nations (Fig. 7). Within the United States, we observed cropland area reduction (<−0.1 Mha) in Texas, Oklahoma, Iowa, and California and an increase (>2 Mha) in Montana and North Dakota. In Canada, no provinces showed a significant reduction of cropland area, but significant gains (>2 Mha) were observed in Manitoba, Alberta, and Saskatchewan.

In Brazil, net cropland change per state ranged from a slight decline in Alagoas (−0.01 Mha) to a major expansion in Mato Grosso (+3.7 Mha). Mato Grosso and Goiás states in particular experienced large gains, driven largely by the expansion of soybean production (Song et al., 2021; Song et al., 2017; Vieira et al., 2022; Zalles et al., 2019). In Argentina, provinces with Pampa (Cordoba and La Pampa) experienced cropland area reduction, while cropland expanded within the Chaco regions (Chaco and Santiago del Estero provinces).

In Europe, Russia and Ukraine led cropland gain during the last decade. In Russia, the largest cropland gain occurred in the steppe regions of the European part of the country, particularly in Saratov, Rostov, and Volgograd regions, each of which gained more than 0.4 Mha. In Ukraine, cropland area increased in regions not directly affected by the war, such as Chernihiv, but decreased in the partly occupied Donetsk region.

In China, cropland change varied widely by region. While Jiangsu lost 0.09 Mha during 2015–2024, Inner Mongolia gained 1.31 Mha of cropland area due to extensive irrigation. In India, cropland gain was concentrated in the country's western drylands, while West Bengal had a small decline (−0.03 Mha). Other significant contributors to cropland dynamics in Asia are Kazakhstan and Pakistan. In Kazakhstan, the largest increase in cropland areas was found in Pavlodar (+0.44 Mha), while in Pakistan, cropland expanded within the dryland regions of Baluchistan and Sindh, driven by irrigation development and canal network extension.

In Australia, the state of South Australia lost 0.1 Mha of cropland area, while cropland area expanded in New South Wales, Queensland, and Western Australia by at least 0.2 Mha each.

3.2. Cropland change trajectories

We analyzed the major trajectories of cropland gain and loss using

Table 3
Continental cropland extent and change area, map-based estimates.

	Cropland 2024, Mha	Percentage of global cropland area	Net cropland change 2003–2015*, Mha	Net cropland change 2015–2024, Mha	Net cropland change 2003–2024, % of 2003 area
Africa	231.2	17.6	31.4	24.5	39.2
Southwest Asia	275.3	21.0	19.4	11.2	13.6
Australia and New Zealand	38.9	3.0	2.4	0.8	7.6
Southeast Asia	210.4	16.0	7.8	5.8	7.8
Europe and North Asia	239.9	18.3	−2.0	10.1	3.5
North and Central America	181.5	13.8	2.2	1.6	1.9
South America	134.2	10.2	27.9	19.9	63.3

* Data from Potapov et al. (2022b).

Table 4
National cropland extent and change area for countries with a 2024 cropland area of at least 20 Mha, map-based estimates.

Country	Cropland 2024, Mha	Percentage of global cropland area	Net cropland change 2003–2015*, Mha	Net cropland change 2015–2024, Mha	Net cropland change 2003–2024, % of 2003
India	152.0	11.6	12.7	5.3	14.9
China	142.7	10.9	3.4	3.4	5.8
United States	128.1	9.8	0.8	−0.1	0.5
Russia	91.5	7.0	−5.8	8.0	2.4
Brazil	70.8	5.4	17.4	16.5	112.8
Argentina	46.8	3.6	6.6	1.0	20.2
Australia	38.4	2.9	2.3	0.9	7.6
Nigeria	38.0	2.9	3.7	2.7	22.5
Canada	36.7	2.8	0.6	1.4	5.5
Ukraine	33.9	2.6	1.0	1.7	8.5
Kazakhstan	25.1	1.9	0.9	2.1	14.4
Ethiopia	22.5	1.7	1.3	1.3	17.8
Sudan	21.7	1.7	2.8	2.4	35.8
Pakistan	20.4	1.6	1.6	1.4	17.8
Tanzania	19.8	1.5	4.1	3.2	76.7

* Data from Potapov et al. (2022b).

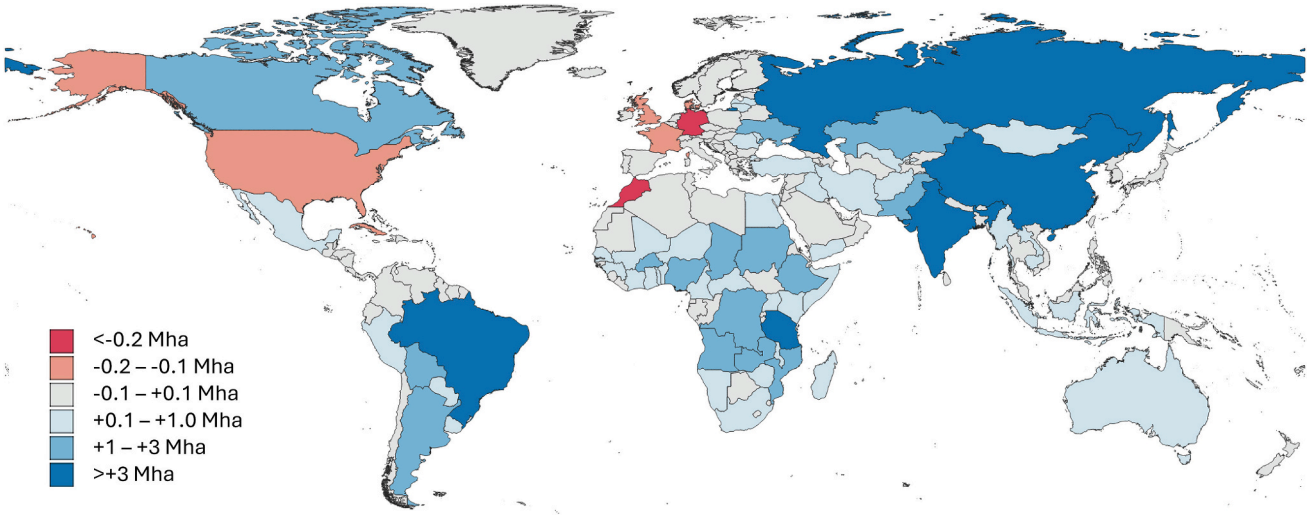

Fig. 4. The net cropland extent changes 2015–2024 per country, map-based estimates (Mha).

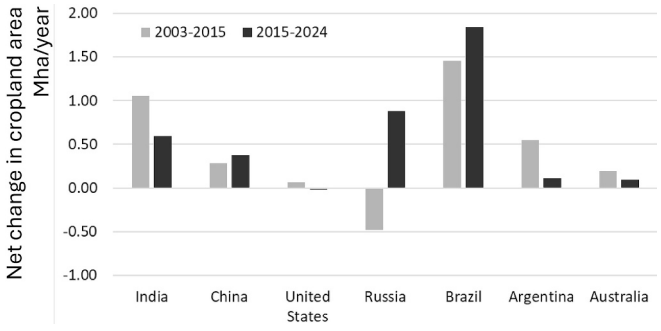

Fig. 5. Net change in national cropland area for countries with the largest year 2024 cropland extent. The 2003–2015 estimate is from Potapov et al. (2022), and the 2015–2024 estimate is from the current research.

reference sample data collected using very high-resolution imagery. To estimate the percentage of the loss and gain area attributed to each trajectory, we used only sample pixels with agreement between the map and reference change detection (e.g., we only estimated cropland gain trajectories for sampled pixels where both map and reference data agreed on the presence of a gain event).

The most common change trajectory for both cropland loss and gain was conversion to or from fallow or pasture (Table 5). For cropland gain, this includes the re-cultivation of previously abandoned cropland and the expansion of crops into former pastures. For cropland loss, that includes conversion to pasture and early stage cropland abandonment, where no transition to another intensive land use was detected. Because our cropland mapping relies on Landsat data aggregated over four years, a conversion to fallow or pasture indicates that the fallow or pasture period exceeded four years, but does not necessarily reflects a permanent change in land use.

A third (33.3%) of all new cropland between 2015 and 2024 was established through natural vegetation clearing or irrigation expansion within natural drylands. This estimate for the 2015–2024 interval is lower than the 48% reported for the 2003–2019 interval (Potapov et al., 2022b). The difference may be due to the widespread abandoned cropland re-cultivation observed in Eastern Europe during the last decade, which increased the share of this change trajectory at the expense of the conversion of natural vegetation. Only a small portion of new croplands replaced agroforestry and tree plantations.

Analyzing the drivers of cropland loss, we found that almost a quarter (24.2%) of cropland was converted to other intensive land uses, including urban areas, infrastructure, aquaculture, and tree crops. Only 8.2% of the cropland loss reverted to natural vegetation, which is smaller than the 16% estimated for the 2003–2019 interval (Potapov

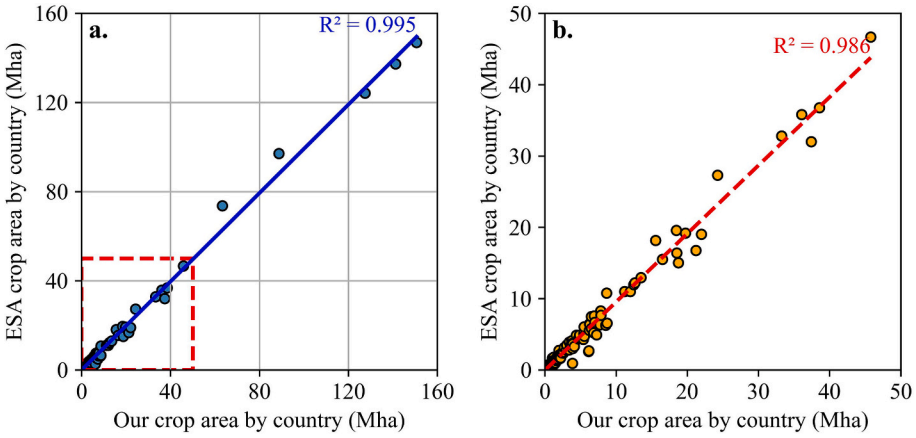

Fig. 6. A comparison between our map-based estimates of national cropland areas for 2021 and the ESA WorldCover 2021 (Zanaga et al., 2022) cropland class extent. a. All countries. b. Countries with cropland extent below 50 Mha.

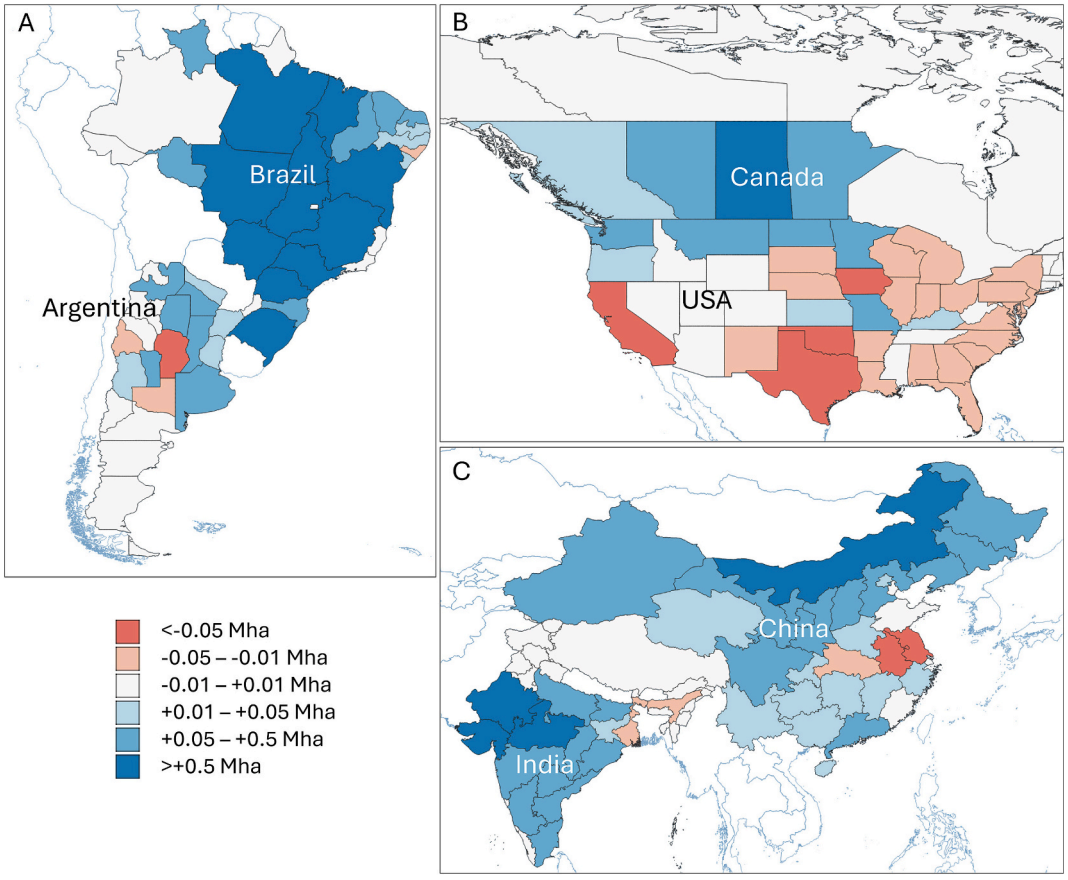

Fig. 7. The net cropland extent changes 2015–2024 per administrative region for selected countries, Mha.

et al., 2022b). This lower proportion may reflect the shorter analysis interval, which provides less time to detect natural vegetation restoration on fallow lands.

4. Discussion

4.1. Advantages and limitations of the annual cropland mapping method

The annual cropland mapping methodology presented here advances our capabilities to produce high cadence, medium spatial resolution datasets that can support land management and food security applications. Efficient and accurate global annual cropland mapping was made possible by regionally and locally calibrated machine learning models, which supported automation of the mapping workflow. Our cropland dataset meets the standards of an essential Landsat data product as outlined by Radeloff et al. (2024) and the sample-based validation confirmed its accuracy. Furthermore, its consistency, transparency, scalability, and accessibility support its potential for operational implementation. We anticipate that our methodology can support the need for operational annual cropland monitoring at global to local spatial scales, providing highly reliable cropland extent and change estimates, while also serving as inputs to applications such as crop type

Table 5
Cropland gain (A) and loss (B) trajectories as estimated from the reference sample data. Standard error of the estimated proportion is provided in parentheses.

A. Cropland gain trajectory	**% total**
*Re*cultivation of a fallow or pasture	61.5 (4.3)
Dryland irrigation	6.3 (2.2)
Replacing trees outside forests	5.2 (1.9)
Natural vegetation conversion	27.0 (4.0)
B. Cropland loss trajectory	**% total**
Conversion to a fallow or pasture	65.4 (5)
Conversion to aquaculture	1.1 (1.1)
Conversion to agroforestry or tree plantation	12.9 (3.5)
Construction or infrastructure expansion	10.2 (3.2)
Flooding	2.2 (1.6)
Abandonment and natural vegetation regrowth	8.2 (3)

mapping, crop irrigation analysis, global crop productivity monitoring, and assessing the impacts of global cropland change on the natural environment.

One objective of our research was to develop an operational annual cropland mapping algorithm. Following the guiding principles for operational products proposed by Radeloff et al. (2024), we employed a well-established analysis-ready satellite data product (GLAD-ARD) and the decision tree ensemble method that has been successfully tested for mapping global land cover (Potapov et al., 2022a, 2022b). We demonstrated the operational capability of the method by applying it for the year 2024. The operationalization of the annual cropland mapping was enabled by radiometrically consistent Landsat GLAD-ARD that provides reliable and consistent annual inputs for global cropland detection models (Section 2.2). The temporal stability of the mapping model was ensured by using calibration data collected from multiple years (Section 2.4). The consistency and continuity of the GLAD-ARD dataset ensure future operational capacity of our cropland mapping method. The accuracy of our cropland dataset has been estimated following good practice recommendations (Olofsson et al., 2014; Tyukavina et al., 2025). Although the accuracy of the 2024 cropland map has not yet been formally assessed, qualitative visual assessment and comparison of annual statistics suggest it is similar to that of the 2015 and 2023 maps. Our source data (GLAD-ARD) and the annual cropland dataset are publicly available without any restrictions on reproduction and use. The annual cropland dataset serves as a core thematic layer for the generation of global land use and land cover products being developed by the GLAD Lab. However, future operational application of our approach depends on public demand for globally consistent land use and food production datasets and, ultimately on the availability of funding to support ongoing updates to meet this demand.

The uncertainty of the cropland reduction and expansion maps (Table 2) suggests that the annual cropland maps have limitations in the detection of changes between the years. Nearly 75% of all errors were due to confusion between croplands, fallows, and pastures, boundary and mixed pixels; and difficulties in mapping rainfed croplands with irregular production cycles. Many of these uncertainties, however, were also present in the high-resolution reference data, highlighting intrinsic limitations of optical imagery. We suggest that some of the issues are scale-dependent and require higher spatial resolution data, such as Sentinel-2 10-m imagery, to improve cropland mapping within smallholder-dominated mosaic landscapes. Other limitations, such as distinguishing intensively managed pastures from annual crops or detecting low-productivity croplands, may require other novel approaches to improve mapping accuracy beyond current machine learning tools and optical satellite data.

4.2. Cropland change drivers

The global cropland map time-series provides insights into some of the major drivers of land use change. We did not perform a quantitative analysis of these drivers. Instead, we provide here a qualitative description of the major drivers that should be investigated further using appropriate data and methods.

At the continental scale, North America has a relatively stable cropland area with marginal changes over the past two decades (Table 3). At the national and sub-national scales, however, we observed substantial changes (Fig. 7B). Cropland area decreased in the Southwest, Southeast, and the southern part of the Great Plains in the USA, while it increased in Canada and in the northern part of the Great Plains (North Dakota and Montana) in the USA. We suggest that the most probable drivers of the observed cropland dynamics were the depletion of the High Plains Aquifer, which limits irrigation in Kansas and Oklahoma (Xie and Lark, 2021), and climate change that benefits crop production in the northern states of the USA and in Canada (Qian et al., 2019). Climate change also affected cropland in Europe, which is well-documented in countries such as Germany (Schmitt et al., 2022).

Brazil featured the largest net cropland area increase of all countries (Table 4), with a large portion of this increase driven by soybean production (Song et al., 2021). The increase in soy cultivation in Latin America, particularly in Brazil, was linked to the soybean price increase in 2022–2023, which is in turn driven by the increased demand for soybeans from China after the country imposed retaliatory tariffs on agricultural exports from the USA in 2018 (Fuchs et al., 2019; Fuchs et al., 2023). Fuchs et al. (2019) predicted that Brazil would need 12.9 Mha more land for cropland production to cover the increasing demand for soybeans from China. From 2019 to 2024, we observed a total cropland extent increase of nearly 12 Mha in Brazil. While not all of the new cropland area is used for soybean production, we suggest that the combined effect of global market disruptions, USA tariff policies, and soybean price increase has driven the acceleration of cropland expansion in Brazil during the past decade.

Cuba stands out as the country with the largest net loss of cropland area from 2003 to 2024 (−0.6 Mha), and a significant (−0.15 Mha) loss during the last decade. We suggest that the collapse of sugar cane production in the country was the primary driver of the observed changes.

While most countries in sub-Saharan Africa feature an increase in cropland area, Morocco presents a significant loss of its croplands (Fig. 8). According to our results, Morocco's cropland extent changed by −0.38 Mha, a 6.0% decline in the country's cropland extent since 2015. We suggest that the observed cropland reduction is associated with the years-long drought (Abdullah, 2024). According to Sara (2024), Morocco's wheat extent and yield have decreased by 50% in 2024, and the country imported 2.5 million tons of wheat in 2023.

Russia represents a unique cropland dynamic over the past decades. While it was ranked as the top country by the cropland reduction from 2003 to 2015 (−5.8 Mha), during the last decade, it gained 8 Mha of cropland area, achieving the second global rank by cropland increase. In particular, winter wheat expanded from 4.71 Mha in 2001 to 8.85 Mha in 2020 (Abys et al., 2024). Following changes in governmental regulations and subsidies aimed at improving food production independence, Russia re-cultivated a large proportion of lands abandoned since the breakdown of the Soviet Union (Deppermann et al., 2018). However, given the international sanctions preventing the trade of fertilizers and seeds, it is unclear whether the increase in cropland area resulted in similar changes in crop yields.

Armed conflicts have a significant impact on land cover and land use, triggering cropland abandonment and reallocation (Baumann and Kuemmerle, 2016). Our analysis of three regions under different types of armed conflicts illustrates their impact on cropland extent change (Fig. 9). In Ukraine, the armed conflict started in 2014 with the occupation of Crimea and separatist war in the eastern part of the country. The war intensified after the Russian full-scale invasion in 2022. The war caused a significant decline in crop production and large-scale cropland abandonment along the frontlines and within the occupied area (Fig. 9A). Previous research estimated the total agriculture abandonment area ranging from 1.7 Mha in 2023 (Hartman et al., 2025) to 2.2

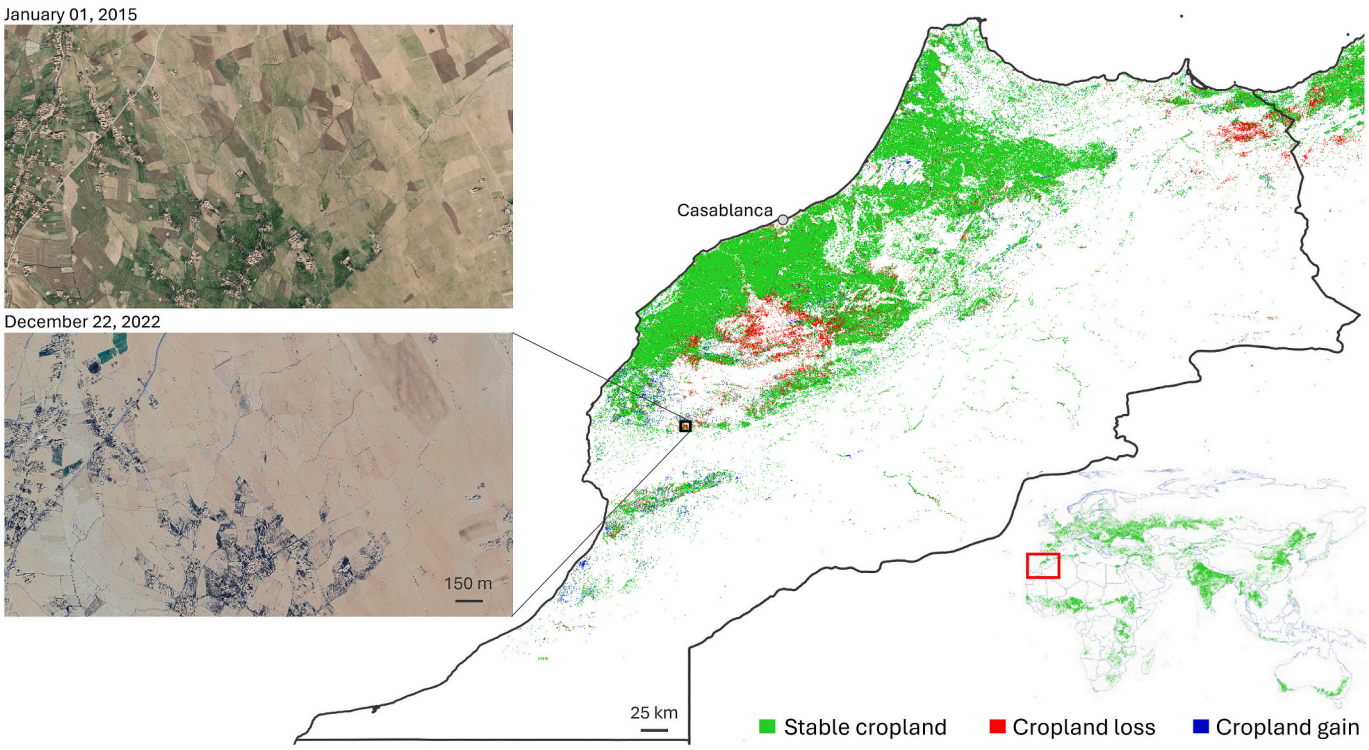

Fig. 8. Cropland loss in Morocco due to years-long drought. A subset of Google Earth imagery illustrates crop failure between 2015 and 2022.

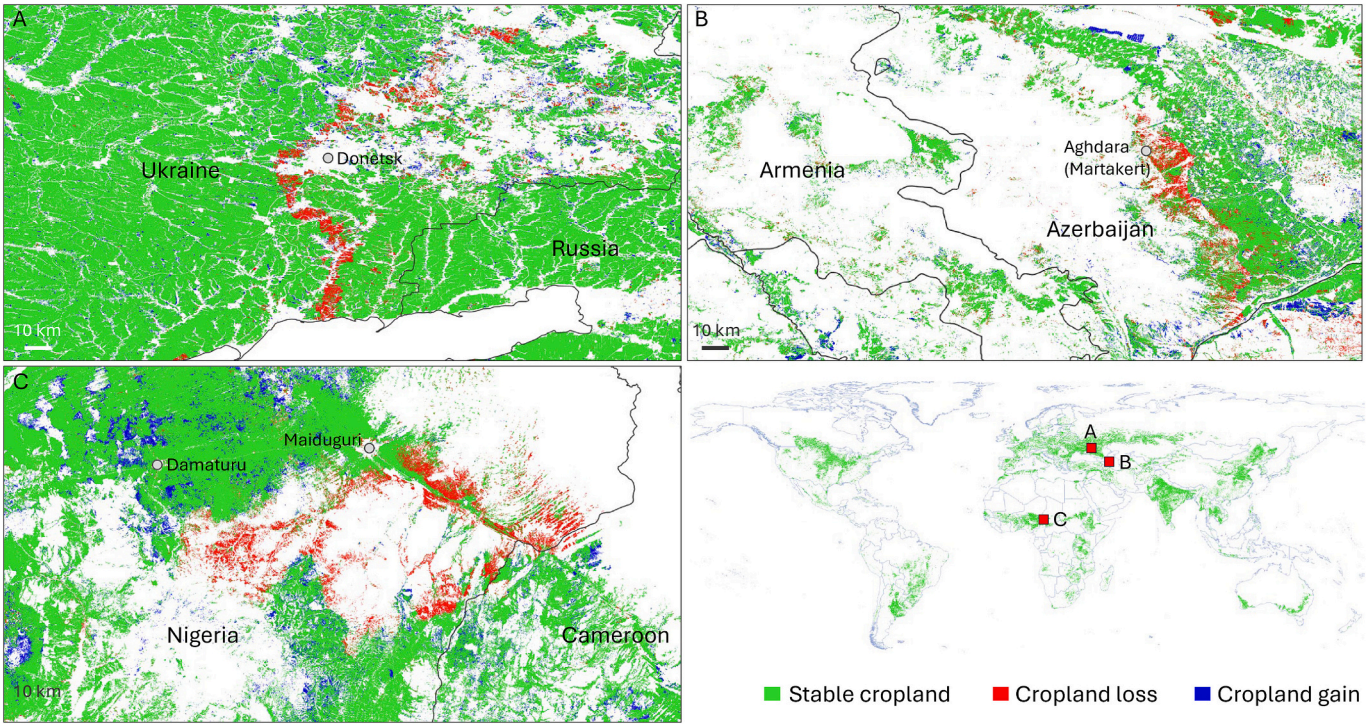

Fig. 9. Examples of cropland change due to armed conflicts in Ukraine (A), Azerbaijan (B), and Nigeria (C).

Mha in 2024 (Wagner et al., 2025). We mapped a smaller area of cropland abandonment of 250,000 ha within the Russia-occupied territory (the occupied territory map was obtained from https://commons.wikimedia.org/w/index.php?curid=115506141). The primary reason for the crop abandonment underestimation by our map is the application of a 4-year maximum fallow length and the aggregation of the Landsat data over a 4-year interval. Our method is not capable of detecting cropland abandonment immediately after the conflict-related cessation of agricultural management. Our results are comparable to the Hartman et al. (2025) estimates of 117,000 ha of fully abandoned cropland area since 2014 and 314,800 ha of emerging cropland abandonment since 2020.

The armed conflict between Azerbaijan and Armenia over the control of the Nagorno-Karabakh region started in the early 1990s, but it intensified after 2015 and eventually led to a massive population displacement. Using the conflict zone map (https://github.com/mkudamatsu/data_karabakh-map), we estimated that from 2015 to 2024, 61,000 ha of cropland (34% total cropland area of the year 2015) have been abandoned within the conflict area (Fig. 9B).

In Nigeria, armed conflict and associated insecurity linked to Boko Haram, together with broader political and social instability, have triggered population displacement that resulted in cropland loss and gain in the north-eastern states of Borno, Adamawa, and Yobe. Boko Haram has operated predominantly in rural areas of Nigeria, where agriculture is a major land use (Pretty, 1999; Adelaja and George, 2019). Conflict induced displacement led to cropland abandonment in affected communities, while agricultural expansion occurred in areas of refugee resettlement. The sharp changes in cropland extent were observed along the provincial boundaries in Nigeria (Fig. 9C), where large areas of cropland were abandoned within Borno province (with provincial capital in Maiduguri) while cropland is expanding at the expense of natural woodlands in the neighboring Yobe province. We estimated that from 2015 to 2024, 314,000 ha of cropland areas in Borno province were abandoned, which represent 20% of the 2015 cropland area.

Commercial and residential construction and infrastructure development are responsible for more than a 10% reduction of the croplands during the last decade (Table 5). Unlike other cropland loss trajectories, construction represents the permanent removal of land from future agricultural production. Growing international trade, and especially the rise in e-commerce, have recently increased the demand for large logistics terminals and distribution centers. Many such facilities were constructed around trade hubs located on road confluences, such as Indianapolis in the USA and Warsaw in Poland. The expansion of warehouses, along with residential construction, contributed to cropland reduction around these cities during the last decade (Fig. 10A-B). The growing population and urbanization in Asia and the demand for expansion in residential built-up areas resulted in cropland reduction in the peripheries of large urban centers (Fig. 10C—D).

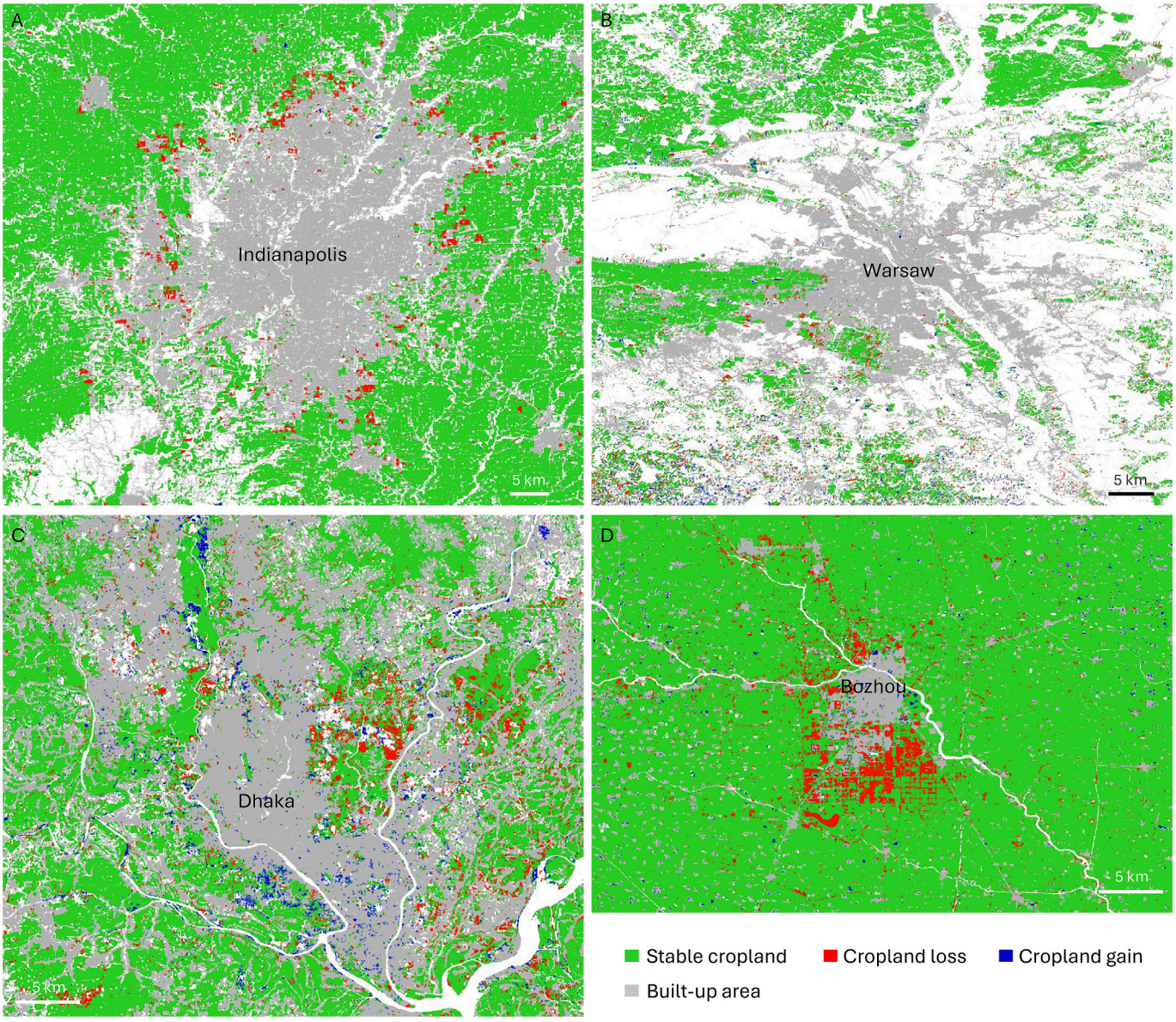

Fig. 10. Examples of cropland conversion to built-up areas around large urban centers: A. Indianapolis, USA; B. Warsaw, Poland; C. Dhaka, Bangladesh; D. Bozhou, China. Built-up areas for the year 2020 are from Potapov et al. (2022a).

4.3. Per capita cropland area

Hunger and food insecurity have worsened since 2015, exacerbated by a combination of factors, including the COVID-19 pandemic, armed conflicts, climate change, and growing environmental and social injustices (Zhao et al., 2025). Against this backdrop, rapid population growth and rising standards of living are exerting immense pressure on limited land resources, including food production. Between 2015 and 2024, against the mapped net change of global cropland area by 6%, the world population grew by 9%. As a result, per-capita cropland declined by 3%, from 0.166 ha per person in 2015 to 0.161 ha per person in 2024. Although rising crop yields may outweigh the per-capita cropland area reduction (Potapov et al., 2022b), our findings suggest that the decline of crop availability may intensify existing food insecurities and shortages if no targeted policy interventions are adopted.

5. Conclusion

During the last decade (2015–2024), global cropland area expanded at an average rate of almost 10 Mha per year. Yet rapid population growth has led to a continuous decline in the global per capita cropland area availability, which poses challenges to food security. Natural disasters, armed conflicts, economic crises and economic expansion with infrastructure development exacerbate risks to global and national food security. The methodology presented here enables annual global cropland monitoring, providing spatiotemporally consistent data on cropland extent that are comparable across political boundaries and relevant at local to global scales. Building on Potapov et al. (2022b), our approach significantly improves both the accuracy and cadence of global cropland mapping. We demonstrated its operational capability by successfully mapping the 2024 cropland extent using pre-trained models. Beyond tracking cropland extent, the annual maps can help us to understand the drivers of cropland change, such as economic factors, climate change, land use policy, and armed conflicts. The annual cropland time-series also provides a framework for further analysis of crop types and productivity, which will be critical for anticipating and addressing food security challenges in the decades ahead.

CRediT authorship contribution statement

Ahmad Khan: Writing – review & editing, Writing – original draft, Visualization, Validation, Investigation, Data curation. **Peter Potapov:** Writing – review & editing, Writing – original draft, Visualization, Validation, Methodology, Data curation, Conceptualization. **Svetlana Turubanova:** Writing – review & editing, Software, Methodology. **Matthew C. Hansen:** Writing – review & editing, Supervision, Project administration, Funding acquisition, Conceptualization. **Alexandra Tyukavina:** Writing – review & editing, Validation. **Andrew Poulson:** Validation. **Andres Hernandez-Serna:** Visualization, Software. **Xiao-Peng Song:** Writing – review & editing. **Nancy Harris:** Writing – review & editing. **Fred Stolle:** Writing – review & editing.

Declaration of competing interest

The authors declare that they have no known competing financial interests or personal relationships that could have appeared to influence the work reported in this paper.

Acknowledgements

This study was supported by the World Resources Institute (WRI) Land & Carbon Lab. Land & Carbon Lab is convened by the WRI and the Bezos Earth Fund. The authors would like to thank Qing Ying (ESSIC UMD), Bernard Adusei (GLAD UMD), and the late Alexander Krylov (former GLAD UMD) for their help with GLAD-ARD production.

Appendix A. Supplementary data

Supplementary data to this article can be found online at https://doi.org/10.1016/j.rse.2026.115438.

Data availability

Landsat analysis-ready data employed in this research are publicly available from https://glad.umd.edu/ard. Annual cropland map data 2015–2024 are publicly available from https://glad.umd.edu/dataset/annual-croplands.

References

Abdullah, S. (2024). Morroco Drought: Satellite Images Show Vital Al Massira Reservoir is Shrinking. BBC News April 9, 2024. Available at https://www.bbc.com/news/world-africa-68665826 https (Accessed: September 30, 2024).
Abys, C., Skakun, S., Becker-Reshef, I., 2024. Two decades of winter wheat expansion and intensification in Russia. Remote Sens. Appl.: Soc. Environ. 33, 101097.
Ackerschott, A., Kohlhase, E., Vollmer, A., Hörisch, J., von Wehrden, H., 2023. Steering of land use in the context of sustainable development: a systematic review of economic instruments. Land Use Policy 129, 106620.
Adelaja, A., George, J., 2019. Terrorism and land use in agriculture: the case of boko haram in Nigeria. Land Use Policy 88, 104116.
Baumann, M., Kuemmerle, T., 2016. The impacts of warfare and armed conflicts on land systems. J. Land Use Sci. 11, 672–688.
Becker-Reshef, I., Justice, C., Vermote, E., Tucker, C., Anyamba, A., Small, J., Pak, E., Masuoka, E., Schmaltz, J., Hansen, M., Pittman, K., Birkett, C., Williams, D., Reynolds, C., Doorn, B., 2010. Monitoring global croplands with coarse resolution earth observations: the global agriculture monitoring (GLAM) project. Remote Sens. 2, 1589–1609.
Becker-Reshef, I., Vermote, E., Lindeman, M., Justice, C., 2010. A generalized regression-based model for forecasting winter wheat yields in Kansas and Ukraine using MODIS data. Remote Sens. Environ. 114, 1312–1323.
Boatwright, G.O., Whitefield, V.S., 1986. Early warning and crop condition assessment research. IEEE Trans. Geosci. Remote Sens. GE-24.
Boryan, C., Yang, Z., Mueller, R., Craig, M., 2011. Monitoring US agriculture: the US department of agriculture, national agricultural statistics service, cropland data layer program. Geocarto Int. 26, 341–358.
Breiman, L., 1996. Bagging predictors. Mach. Learn. 24, 123–140.
Cao, B., Yu, L., Li, X., Chen, M., Li, X., Hao, P., Gong, P., 2021. A 1 km global cropland dataset from 10 000 BCE to 2100 CE. Earth Syst. Sci. Data 13, 5403–5421.
Carlson, K.M., Gerber, J.S., Mueller, N.D., Herrero, M., MacDonald, G.K., Brauman, K.A., Havlik, P., O'Connell, C.S., Johnson, J.A., Saatchi, S., West, P.C., 2017. Greenhouse gas emissions intensity of global croplands. Nat. Clim. Chang. 7, 63–68.
Chen, B., Tu, Y., An, J., Wu, S., Lin, C., Gong, P., 2024. Quantification of losses in agriculture production in eastern Ukraine due to the Russia-Ukraine war. Commun. Earth Environ. 5, 336.
Coulter, L.L., Stow, D.A., Tsai, Y.-H., Ibanez, N., Shih, H.-C., Kerr, A., Benza, M., Weeks, J.R., Mensah, F., 2016. Classification and assessment of land cover and land use change in southern Ghana using dense stacks of landsat 7 ETM+ imagery. Remote Sens. Environ. 184, 396–409.
DeFries, R.S., Foley, J.A., Asner, G.P., 2004. Land-use choices: balancing human needs and ecosystem function. Front. Ecol. Environ. 2, 249–257.
Deppermann, A., Balkovič, J., Bundle, S.-C., Di Fulvio, F., Havlik, P., Leclère, D., Lesiv, M., Prishchepov, A.V., Schepaschenko, D., 2018. Increasing crop production in Russia and Ukraine—regional and global impacts from intensification and recultivation. Environ. Res. Lett. 13, 025008.
DeVries, B., Pratihast, A.K., Verbesselt, J., Kooistra, L., Herold, M., 2016. Characterizing forest change using community-based monitoring data and landsat time series. PLoS ONE 11, e0147121.
Erickson, J.D., 1984. The LACIE experiment in satellite aided monitoring of global crop production. In: Goodwell, G.M. (Ed.), The Role of Terrestrial Vegetation in the Global Carbon Cycle: Measurement by Remote Sensing. John Wiley & Sons Ltd, New York, USA, pp. 191–217.
Evans, A. (2009). The Feeding of the Nine Billion: Global Food Security for the 21st Century. Chatham House, London: The Royal Institute of International Affairs.
FAO, 2005. A System of Integrated Agricultural Censuses and Surveys. Volume 1. World Programme for the Census of Agriculture, Rome, Italy.
FAO, 2024. Gloobal, Regional and Country Trends. FAOSTAT Analytical Briefs: Food and Agriculture Organization of the United Nations, Rome, Italy.
FAO, 2025. FAOSTAT: Food and Agriculture Data. Food and Agriculture Organization of the United Nations, Rome, Italy.
Foley, J.A., DeFries, R., Asner, G.P., Barford, C., Bonan, G., Carpenter, S.R., Chapin, F.S., Coe, M.T., Daily, G.C., Gibbs, H.K., Helkowski, J.H., Holloway, T., Howard, E.A., Kucharik, C.J., Monfreda, C., Patz, J.A., Prentice, I.C., Ramankutty, N., Snyder, P.K., 2005. Global consequences of land use. Science 309, 570–574.
Foley, J.A., Ramankutty, N., Brauman, K.A., Cassidy, E.S., Gerber, J.S., Johnston, M., Mueller, N.D., O'Connell, C., Ray, D.K., West, P.C., Balzer, C., Bennett, E.M., Carpenter, S.R., Hill, J., Monfreda, C., Polasky, S., Rockström, J., Sheehan, J., Siebert, S., Tilman, D., Zaks, D.P.M., 2011. Solutions for a cultivated planet. Nature 478, 337–342.

Friedl, M.A., Sulla-Menashe, D., Tan, B., Schneider, A., Ramankutty, N., Sibley, A., Huang, X., 2010. MODIS collection 5 global land cover: algorithm refinements and characterization of new datasets. Remote Sens. Environ. 114, 168–182.
Fuchs, R., Alexander, P., Brown, C., Cossar, F., Henry, R.C., Rounsevell, M., 2019. Why the US-China trade war spells disaster for the amazon. Nature 567, 451–454.
Fuchs, R., Raymond, J., Winkler, K., Rounsevell, M., 2023. Short-sighted policies are fuelling Brazilian deforestation. Nature 624, 522.
Gao, B., 1996. NDWI - a normalized difference water index for remote sensing of vegetation liquid water from space. Remote Sens. Environ. 58 (3), 258–266.
Gibbs, H.K., Ruesch, A.S., Achard, F., Clayton, M.K., Holmgren, P., Ramankutty, N., Foley, J.A., 2010. Tropical forests were the primary sources of new agricultural land in the 1980s and 1990s. Proc. Natl. Acad. Sci. 107, 16732–16737.
Godfray, H.C., Beddington, J.R., Crute, I.R., Haddad, L., Lawrence, D., Muir, J.F., Pretty, J., Robinson, S., Thomas, S.M., Toulmin, C., 2010. Food security: the challenge of feeding 9 billion people. Science 327, 812–818.
Haberl, H., Erb, K.H., Krausmann, F., Gaube, V., Bondeau, A., Plutzar, C., Gingrich, S., Lucht, W., Fischer-Kowalski, M., 2007. Quantifying and mapping the human appropriation of net primary production in earth's terrestrial ecosystems. Proc. Natl. Acad. Sci. 104, 12942–12947.
Hansen, M.C., DeFries, R.S., Townshend, J.R., Sohlberg, R., 2000. Global land cover classification at 1 km spatial resolution using a classification tree approach. Int. J. Remote Sens. 21, 1331–1364.
Hartman, S., Whiteside, R., Smaliychuk, A., Dronova, I., 2025. Land abandonment as an indicator of Ukrainian agricultural resilience during Russias war against Ukraine. Appl. Geogr. 183, 103744. https://doi.org/10.1016/j.apgeog.2025.103744.
Heilmayr, R., Rausch, L.L., Munger, J., Gibbs, H.K., 2020. Brazils amazon soy moratorium reduced deforestation. Nat. Food 1, 801–810.
Jarvis, A., Reuter, H.I., Nelson, A., Guevara, E., 2008. Hole-Filled Seamless SRTM Data v4 [Dataset]. International center for tropical, & agriculture (CIAT). http://srtm.csi.cgiar.org.
Lambin, E.F., Meyfroidt, P., 2011. Global land use change, economic globalization, and the looming land scarcity. Proc. Natl. Acad. Sci. 108, 3465–3472.
Loveland, T.R., Reed, B.C., Brown, J.F., Ohlen, D.O., Zhu, Z., Yang, L., Merchant, J.W., 2000. Development of a global land cover characteristics database and IGBP DISCover from 1 km AVHRR data. Int. J. Remote Sens. 21, 1303–1330.
Nellemann, C., MacDevette, M., Manders, T., Eickhout, B., Svilhus, B., Prins, A.G., Kalltenborn, B.P., 2009. The Environmental Food Crisis - the Environment's Role in Averting Future Food Crisis: a UNEP Rapid Response Assessment. United Nations Environment Programme (UNEP) and GRID-Arendal, Nairobi, Kenya. Available at: www.grida.no (Accessed October 15, 2025).
Olofsson, P., Arévalo, P., Espejo, A.B., Green, C., Lindquist, E., McRoberts, R.E., Sanz, M. J., 2020. Mitigating the effects of omission errors on area and area change estimates. Remote Sens. Environ. 236, 111492.
Olofsson, P., Foody, G.M., Herold, M., Stehman, S.V., Woodcock, C.E., Wulder, M.A., 2014. Good practices for estimating area and assessing accuracy of land change. Remote Sens. Environ. 148, 42–47.
Pittman, K., Hansen, M., Becker-Reshef, I., Potapov, P.V., Justice, C.P., 2010. Estimating global cropland extent with multi-year MODIS data. Remote Sens. 2, 20.
Potapov, P., Hansen, M.C., Kommareddy, I., Kommareddy, A., Turubanova, S., Pickens, A., Adusei, B., Tyukavina, A., Ying, Q., 2020. Landsat analysis ready data for global land cover and land cover change mapping. Remote Sens. 12.
Potapov, P., Li, X., Hernandez-Serna, A., Tyukavina, A., Hansen, M.C., Kommareddy, A., Pickens, A., Turubanova, S., Tang, H., Silva, C.E., Armston, J., Dubayah, R., Blair, J. B., Hofton, M., 2021. Mapping global forest canopy height through integration of GEDI and landsat data. Remote Sens. Environ. 253, 112165.
Potapov, P., Hansen, M.C., Pickens, A., Hernandez-Serna, A., Tyukavina, A., Turubanova, S., Zalles, V., Li, X., Khan, A., Stolle, F., Harris, N., Song, X.-P., Baggett, A., Kommareddy, I., Kommareddy, A., 2022a. The global 2000-2020 land cover and land use change dataset derived from the Landsat archive: first results. Front. Remote Sens. 3.
Potapov, P., Turubanova, S., Hansen, M.C., Tyukavina, A., Zalles, V., Khan, A., Song, X.-P., Pickens, A., Shen, Q., Cortez, J., 2022b. Global maps of cropland extent and change show accelerated cropland expansion in the twenty-first century. Nat. Food 3, 19–28.
Potapov, P., Hansen, M.C., Turubanova, S., Tyukavina, A., Zalles, V., Song, X.-P., Khan, A., 2023. Reply to: measuring the world's cropland area. Nat. Food 4, 33–34.
Pretty, J., 1999. Can sustainable agriculture feed Africa? New evidence on progress, processes and impacts. Dev. Sustain. 1, 253–274. https://doi.org/10.1023/A:1010039224868.
Prishchepov, A.V., Müller, D., Dubinin, M., Baumann, M., Radeloff, V.C., 2013. Determinants of agricultural land abandonment in post-soviet european Russia. Land Use Policy 30, 873–884.
Qian, B., Zhang, X., Smith, W., Grant, B., Jing, Q., Cannon, A.J., Neilsen, D., McConkey, B., Li, G., Bonsal, B., Wan, H., Xue, L., Zhao, J., 2019. Climate change impacts on Canadian yields of spring wheat, canola and maize for global warming levels of 1.5°c, 2.0°c, 2.5°c and 3.0°c. Environ. Res. Lett. 14, 074005.
Radeloff, V.C., Roy, D.P., Wulder, M.A., Anderson, M., Cook, B., Crawford, C.J., Friedl, M., Gao, F., Gorelick, N., Hansen, M., Healey, S., Hostert, P., Hulley, G., Huntington, J.L., Johnson, D.M., Neigh, C., Lyapustin, A., Lymburner, L., Pahlevan, N., Pekel, J.F., Scambos, T.A., Schaaf, C., Strobl, P., Woodcock, C.E., Zhang, H.K., Zhu, Z., 2024. Need and vision for global medium-resolution landsat and sentinel-2 data products. Remote Sens. Environ. 300.
Ramankutty, N., Foley, J.A., 1998. Characterizing patterns of global land use: an analysis of global croplands data. Glob. Biogeochem. Cycles 12, 667–685.
Ramankutty, N., Evan, A.T., Monfreda, C., Foley, J.A., 2008. Farming the planet: 1. Geographic distribution of global agricultural lands in the year 2000. Glob. Biogeochem. Cycles 22.
Rembold, F., Meroni, M., Urbano, F., Lemoine, G., Kerdiles, H., Perez-Hoyos, A., Csak, G., 2017. ASAP - anomaly hot spots of agricultural production, a new early warning decision support system developed by the joint research Centre. In: Proceedings of the 9th International Workshop on the Analysis of Multitemporal Remote Sensing Images (MultiTemp), pp. 1–5.
Reynolds, C., 2001. Input data Sources, Climate Normals, Crop Models, and Data Extraction Routines Utilized by OGA/IPAD. Third International Conference on Geospatial Information in Agriculture and Forestry, Denver, Colorado.
Sara, R., 2024. Prolonged Drought in Morocco Slashes 2024 Wheat Harvest by Nearly 50%: Innovative Solutions in the Face of Crisis. United Nations Convention to Combat Desertification (UNCCD).
Schmitt, J., Offermann, F., Söder, M., Frühauf, C., Finger, R., 2022. Extreme weather events cause significant crop yield losses at the farm level in German agriculture. Food Policy 112, 102359.
Song, X.-P., Potapov, P.V., Krylov, A., King, L., Di Bella, C.M., Hudson, A., Khan, A., Adusei, B., Stehman, S.V., Hansen, M.C., 2017. National-scale soybean mapping and area estimation in the United States using medium resolution satellite imagery and field survey. Remote Sens. Environ. 190, 383–395.
Song, X.-P., Hansen, M.C., Potapov, P., Adusei, B., Pickering, J., Adami, M., Lima, A., Zalles, V., Stehman, S.V., Di Bella, C.M., Conde, M.C., Copati, E.J., Fernandes, L.B., Hernandez-Serna, A., Jantz, S.M., Pickens, A.H., Turubanova, S., Tyukavina, A., 2021. Massive soybean expansion in South America since 2000 and implications for conservation. Nat. Sustainability 4, 784–792.
Thenkabail, P.S., Teluguntla, P.G., Xiong, J., Oliphant, A., Congalton, R.G., Ozdogan, M., Gumma, M.K., Tilton, J.C., Giri, C., Milesi, C., Phalke, A., Massey, R., Yadav, K., Sankey, T., Zhong, Y., Aneece, I., & Foley, D. (2021). Global Cropland-Extent Product at 30-m Resolution (GCEP30) Derived From Landsat Satellite Time-Series Data for the Year 2015 Using Multiple Machine-Learning Algorithms on Google Earth Engine Cloud, Reston, VA. Paper (p. 63).
Tilman, D., Balzer, C., Hill, J., Befort, B.L., 2011. Global food demand and the sustainable intensification of agriculture. Proc. Natl. Acad. Sci. 108, 20260–20264.
Tucker, C.J., 1979. Photographic infrared linear combinations for monitoring vegetation. Remote Sens. Environ. 8 (2), 127–150.
Tyukavina, A., Stehman, S.V., Pickens, A.H., Potapov, P., Hansen, M.C., 2025. Practical global sampling methods for estimating area and map accuracy of land cover and change. Remote Sens. Environ. 324, 114714.
USDA, 2025. Cropland Data Layer. National Agricultural Statistics Service (NASS), U.S. Department of Agriculture. Available at https://croplandcros.scinet.usda.gov/. Accessed: June 15, 2025.
USGS, 2023. Global Food Security-Support analysis Data at 30m (GFSAD) [Dataset]. https://www.usgs.gov/centers/western-geographic-science-center/science/global-food-and-water-security-support-analysis.
Van Deventer, A.P., Ward, A.D., Gowda, P.H., Lyon, J.G., 1997. Using thematic mapper data to identify contrasting soil plains and tillage. Photogramm. Eng. Remote. Sens. 63, 87–93.
Vieira, D.C., Sanches, I.D.A., Montibeller, B., Prudente, V.H.R., Hansen, M.C., Baggett, A., Adami, M., 2022. Cropland expansion, intensification, and reduction in Mato Grosso state, Brazil, between the crop years 2000/01 to 2017/18. Remote Sens. Appl.: Soc. Environ. 28, 100841.
Wagner, J., Nair, S.S., Skakun, S., Duncan, E.C., Li, F., Oliinyk, O., Nerry, F., Rehbinder, J., Becker-Reshef, I., 2025. Monitoring cropland cultivation, abandonment, fallowing and recultivation dynamics with regard to conflict intensity in war-affected Ukraine. Sci. Remote Sens. 12, 100326. https://doi.org/10.1016/j.srs.2025.100326.
Walker, R., 2011. The impact of Brazilian biofuel production on Amazônia. Ann. Assoc. Am. Geogr. 101, 929–938.
World Bank, 2011. Global Strategy to Improve Agricultural and Rural Statistics: Report of the Friends of the Chair on Agricultural Statistics. The World Bank, Washington D. C, p. 55.
World Bank, . World Bank Open Data. https://data.worldbank.org/:. The World Bank Group, Washington D. C.
WorldBank, 2023. In: The World Bank (Ed.), Development Indicators. https://data.worldbank.org/indicator/SP.POP.TOTL:.
Wu, B., Meng, U., Li, Q., Yan, N., Du, X., Zhang, M., 2014. Remote sensing-based global crop monitoring: experiences with Chinas CropWatch system. Int. J. Digit. Earth 7 (2), 113–137. https://doi.org/10.1080/17538947.2013.821185.
Xie, Y., Lark, T.J., 2021. Mapping annual irrigation from landsat imagery and environmental variables across the conterminous United States. Remote Sens. Environ. 260, 112445.
Yu, L., Wang, J., Clinton, N., Xin, Q., Zhong, L., Chen, Y., Gong, P., 2013. FROM-GC: 30 m global cropland extent derived through multisource data integration. Int. J. Digit. Earth 6, 521–533.
Zalles, V., Hansen, M.C., Potapov, P.V., Stehman, S.V., Tyukavina, A., Pickens, A., Song, X.P., Adusei, B., Okpa, C., Aguilar, R., John, N., Chavez, S., 2019. Near doubling of Brazil's intensive row crop area since 2000. Proc. Natl. Acad. Sci. USA 116, 428–435.
Zanaga, D., Van De Kerchove, R., Daems, D., De Keersmaecker, W., Brockmann, C., Kirches, G., Wevers, J., Cartus, O., Santoro, M., Fritz, S., Lesiv, M., Herold, M.,

Tsendbazar, N.E., Xu, P., Ramoino, F., Arino, O., 2022. ESA WorldCover 10 m 2021 v200. Zenodo. https://doi.org/10.5281/zenodo.7254221.

Zhang, C., Kerner, H., Wang, S., Hao, P., Li, Z., Hunt, K.A., Abernethy, J., Zhao, H., Gao, F., Di, L., Guo, C., Liu, Z., Yang, Z., Mueller, R., Boryan, C., Chen, Q., Beeson, P. C., Zhang, H.K., Shen, Y., 2025. Remote sensing for crop mapping: a perspective on current and future crop-specific land cover data products. Remote Sens. Environ. 330, 114995.

Zhao, T., Zhang, X., Liu, W., Wang, J., Li, Z., Liu, L., 2025. Increase in per capita cropland imbalance across countries from 1985 to 2022: a threat to achieving sustainable development goals. Geograph. Sustain. 6, 100239.